Retrieval of Model Initial Fields from Single-Doppler Observations of a Supercell Thunderstorm. Part I: Single-Doppler Velocity Retrieval

STEPHEN S. WEYGANDT,* ALAN SHAPIRO, AND KELVIN K. DROEGEMEIER

Center for Analysis and Prediction of Storms, and School of Meteorology, University of Oklahoma, Norman, Oklahoma

(Manuscript received 23 February 2001, in final form 30 July 2001)

ABSTRACT

In this two-part study, a single-Doppler parameter retrieval technique is developed and applied to a real-data case to provide initial conditions for a short-range prediction of a supercell thunderstorm. The technique consists of the sequential application of a single-Doppler velocity retrieval (SDVR), followed by a variational velocity adjustment, a thermodynamic retrieval, and a moisture specification step. By utilizing a sequence of retrievals in this manner, some of the difficulties associated with full-model adjoints (possible solution nonuniqueness and large computational expense) can be circumvented. In Part I, the SDVR procedure and present results from its application to a deep-convective storm are discussed. Part II focuses on the thermodynamic retrieval and subsequent numerical prediction.

For the SDVR, Shapiro's reflectivity conservation-based method is adapted by applying it in a moving reference frame. Verification of the retrieved wind fields against corresponding dual-Doppler analyses indicates that the best skill scores are obtained for a reference frame moving with the mean wind, which effectively reduces the problem to a perturbation retrieval. A decomposition of the retrieved wind field into mean and perturbation components shows that the mean wind accounts for a substantial portion of the total retrieved azimuthal velocity. At low levels, where the retrieval skill scores are especially good, the retrieved perturbation azimuthal velocity is mostly associated with the polar component of vorticity. Missing from the retrieved fields (compared to the dual-Doppler analysis) is most of the low-level azimuthal convergence. Consistent with this result, most of the retrieved updraft is associated with convergence of the perturbation radial velocity, which is calculated from the observed radial velocity and directly used in the wind retrieval.

1. Introduction

The installation of the Weather Surveillance Radar-1988 Doppler network (WSR-88D; Klazura and Imy 1993) combined with continual increases in computer power have heightened prospects for the operational implementation of numerical models designed to explicitly predict the evolution of individual thunderstorms and their larger aggregates (Lilly 1990; Droegemeier 1990, 1997). Toward that end, a significant research effort has focused on the development of numerical analysis and prediction techniques suitable for convective-scale phenomena and observing systems.

Because Doppler radars are at present the only observing system capable of sampling the detailed flow patterns within thunderstorms and because the large distance between WSR-88D radars generally precludes multiple Doppler wind syntheses, much of the research effort has focused on retrieving initial forecast fields from single-Doppler radar observations. As discussed by Crook (1994), two basic methodologies have been employed: those that retrieve all unobserved fields simultaneously and those that retrieve the three-dimensional wind first, followed by a retrieval of the thermodynamic fields.

The usual approach for retrieving all fields simultaneously has been to fit a numerical model to a time series of observations using four-dimensional variational (4DVAR) techniques. The 4DVAR approach has many advantages and has become increasingly popular in recent years. The advantages include use of the full-model equations as constraints, simultaneous use of all observations in their raw form, provision for inclusion of error covariance information, and the ability to retrieve unobserved fields and find optimal values for model parameters. The 4DVAR approach may be especially useful for storm-scale retrieval, because it provides potentially the best link between the model-predicted fields and the observations.

The 4DVAR technique was originally developed for simple models (Lewis and Derber 1985; LeDimet and Talagrand 1986; Talagrand and Courtier 1987) and then

* Current affiliation: NOAA Office of Atmospheric Research, Forecast Systems Laboratory, Boulder, Colorado.

Corresponding author address: Stephen S. Weygandt, NOAA Forecast Systems Laboratory, 325 Broadway, R/FS1, Boulder, CO 80305-3328.
E-mail: weygandt@fsl.noaa.gov

applied to the problem of initializing large-scale numerical models (Navon et al. 1992; Zupanski 1993; Thepaut et al. 1993; Zou et al. 1993). Sun et al. (1991) were the first to successfully apply the adjoint technique to the single-Doppler retrieval problem. Using a dry Boussinesq model of horizontally periodic Rayleigh convection, they retrieved wind and thermodynamic fields from a single Cartesian velocity component. Real-data tests by Sun and Crook (1994) produced good results for a dry gust-front case. More recently, Sun and Crook (1997, 1998) tested a moist version of their adjoint retrieval model using both simulated and real radar data observations of a deep-convective storm.

Despite the encouraging results obtained in these studies, a number of difficulties have precluded operational implementation of an adjoint-based model initialization procedure for deep-convective storms. First, the severe underdeterminancy and strong nonlinearity of the problem may make it difficult to obtain a unique, converged solution. Second, the many nondifferentiable ''on/off'' switches found in moist physical parameterizations complicate the construction of accurate tangent linear and adjoint models (Xu 1996). Third, use of the full-model equations as a strong constraint neglects the model error. Finally, the computational expense of numerical descent algorithms for finding the minimum of the cost function is still prohibitive for real-time applications to deep-convective storms.

The second methodology for obtaining model initial fields from single-Doppler radar observations involves the sequential application of a three-dimensional single-Doppler velocity retrieval (SDVR) followed by a thermodynamic retrieval. By applying variational wind and thermodynamic retrievals in a sequential manner, it may be possible to circumvent some of the difficulties associated with the full-model adjoint techniques, while still retaining many of their attributes, including the use of dynamic constraints and time-tendency information.

Over the past two decades, a number of methods for retrieving spatially varying wind vectors from a series of radar observations have been developed. Early work focused on techniques for objectively determining the motion of reflectivity or radial velocity features appearing in successive radar scans (Rhinehart 1979; Smythe and Zrnic 1983; Tuttle and Foote 1990). Implicit in these techniques was an assumption of reflectivity or radial velocity conservation. More recent techniques have utilized a variety of assumptions, including satisfaction of simplified prognostic equations for reflectivity or radial velocity, mass conservation, spatial smoothness, velocity stationarity, and frozen turbulence (velocity stationarity in a moving reference frame) enforced as either strong or weak constraints (Qiu and Xu 1992; Xu et al. 1994a,b, 1995; Laroche and Zawadzki 1994, 1995; Shapiro et al. 1995a; Zhang and Gal-Chen 1996; Xu et al. 2001; Gao et al. 2001).

Another broad class of retrieval procedures has dealt with the problem of diagnosing thermodynamic fields from a time history of wind data. Gal-Chen (1978) and Hane and Scott (1978) described a least squares technique that obtains pressure deviations from a horizontal average using the horizontal momentum equations as weak constraints. Buoyancy perturbations are then obtained from the retrieved pressure field using the vertical momentum equation. Unfortunately, this technique cannot be used to obtain fields of total pressure and buoyancy unless a column of independent values is available for either pressure or buoyancy. A further limitation of the procedure for deep-convective storms is that the temperature field cannot be obtained from the buoyancy field unless the moisture fields are known. Inclusion of a thermodynamic equation in the retrieval (Roux 1985) overcomes the first difficulty, but requires an estimate of the time tendency of the temperature field. Sun and Crook (1996) demonstrated that for dry gust-front cases the retrieval of thermodynamic fields from a time series of three-dimensional wind fields could also be accomplished using 4DVAR techniques.

In addition to wind and thermodynamic retrievals, procedures have been developed to estimate microphysical parameters from Doppler radar data. Typically they have relied on the availability of a known three-dimensional wind field, such as that obtained from a multiple-Doppler wind analysis. Rutledge and Hobbs (1983, 1984) and Ziegler (1985, 1988) independently developed techniques in which conservation equations for heat and moisture were integrated forward toward a steady state using a prescribed time-invariant wind field. Hauser and Amayenc (1986) inverted steady-state forms of the conservation equations to obtain microphysical fields. Verlinde and Cotton (1990) documented some of the limitations of the steady-state assumption and later avoided it by fitting a fully time-dependent kinematic model to idealized observations using the adjoint technique (Verlinde and Cotton 1993).

Lin et al. (1993) obtained initial forecast fields for the 20 May 1977 Del City, Oklahoma, tornado case (Ray et al. 1981) by applying a thermodynamic retrieval to dual-Doppler–derived three-dimensional wind fields and making some simple assumptions about the microphysical variables. Time tendencies of the velocity fields were neglected in the thermodynamic retrieval and retrieved thermodynamic fields were retained within regions of hole-filled velocity data. A short-range numerical prediction initialized from the retrieved fields was found to evolve faster than the observed storm. Crook and Tuttle (1994) describe a single-Doppler initialization procedure that combines the tracking reflectivity echoes by correlation wind retrieval (TREC; Rhinehart 1979) with a thermodynamic retrieval. Use of their procedure to initialize three short-range model predictions of dry high plains gust fronts resulted in a modest improvement over a persistence forecast.

In essence, this study extends the work of Lin et al.

(1993) to single-Doppler observations by replacing the second set of radar observations with an SDVR procedure and extends the work of Crook and Tuttle (1994) by considering a deep-convective storm as opposed to a dry microburst case. As such, it, along with the related work of Lazarus (1996) and a full-model adjoint case reported by Wilson et al. (1998), represent the only reported attempts to perform a real-data explicit numerical thunderstorm prediction from initial conditions derived from single-Doppler observations.

In this study, we utilize the ''two-scalar'' wind retrieval described by Shapiro et al. (1995a), applied in a moving reference frame, to obtain three-dimensional velocity vectors within a deep-convective storm volume. A slightly modified version of Gal-Chen's (1978) thermodynamic retrieval procedure (Shapiro and Lazarus 1993) is then used to obtain the pressure and temperature fields from the retrieved three-dimensional wind vectors. Simple assumptions (similar to those employed by Lin et al. 1993) are used to obtain initial moisture fields.

In Part I of this study, we describe the application of the wind retrieval to a deep-convective storm and present a detailed analysis of the retrieved wind fields. In Weygandt et al. (2002, hereafter Part II), we describe the remainder of the retrieval procedure (variational wind adjustment, thermodynamic retrieval, and moisture specification) and report on retrieval results and numerical prediction experiments using the Advanced Regional Prediction System (ARPS; Xue et al. 1995, 2000, 2001). The organization of Part I is as follows. In section 2, we summarize the entire initialization procedure and present a detailed description of the wind retrieval. In section 3, we summarize the supercell thunderstorm radar dataset used for this study, and its processing. In section 4, we show wind retrieval results for both the fixed and moving reference frame experiments. Next, a detailed analysis and decomposition of the retrieved wind field is presented in section 5. We then summarize our results and discuss their implications in section 6.

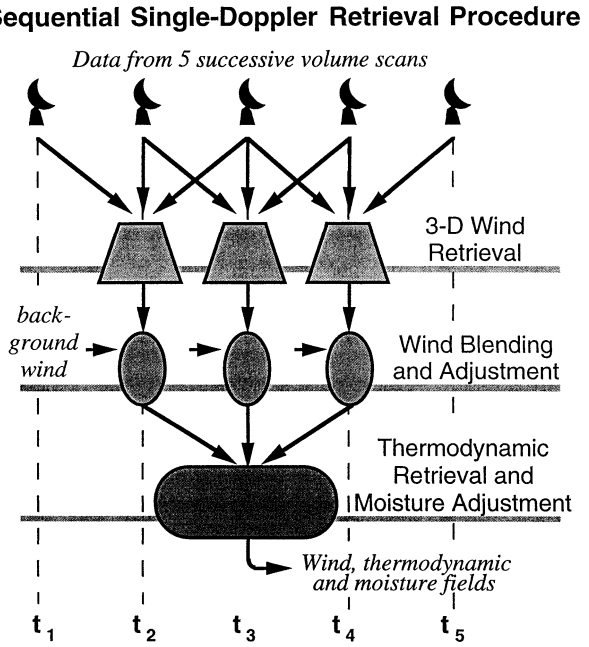

FIG. 1. Flow chart illustrating the sequential single-Doppler retrieval procedure. Five successive single-Doppler volume scans are used to create 3D wind fields at three successive times. The retrieved wind fields are then blended with a background field and variationally adjusted. Finally, thermodynamic fields for the middle time level are retrieved from the three sets of adjusted wind fields and the moisture fields are specified.

2. Retrieval procedure

The sequential single-Doppler retrieval procedure includes two primary components. The first is a single-Doppler velocity retrieval designed to deduce the unobserved cross-beam wind (azimuthal and polar components) from a time series of single-Doppler observations (reflectivity and radial velocity data). The second is a thermodynamic retrieval, which obtains the temperature and pressure fields from a time series of three-dimensional wind fields. Three additional steps are also included in the procedure: a simple algorithm for blending the radar-retrieved winds with background winds, a variational adjustment of the blended wind field to satisfy mass conservation and the observed radial velocity on the model grid, and a moisture specification step.

A flow chart illustrating the entire procedure is shown in Fig. 1. Note that the SDVR used in this study requires three successive single-Doppler volume scans so that centered time differences can be evaluated at the middle time level. Three successive applications of the wind retrieval (utilizing a total of five successive volume scans) yield the three successive three-dimensional wind estimates required to calculate centered time derivatives for the thermodynamic retrieval. A detailed description of the single-Doppler wind retrieval is given in Shapiro et al. (1995a), so here we only summarize it, then describe techniques for applying it in a moving reference frame. Description of the other retrieval components is deferred to Part II of this study.

a. Formulation of the wind retrieval

The two-scalar wind retrieval described by Shapiro et al. (1995a) obtains estimates of the two unobserved spherical wind components (azimuthal and spherical polar) throughout a three-dimensional storm volume from a sequence of three single-Doppler volume scans (reflectivity and radial velocity). One advantage of the two-scalar technique is that it directly obtains the three-dimensional wind field. Many SDVR algorithms obtain only the horizontal wind field (Tuttle and Foote 1990;

Xu et al. 1994a,b; Laroche and Zawadzki 1995; Zhang and Gal-Chen 1996) necessitating a separate vertical integration of the horizontal divergence to obtain vertical velocity. More recently, Xu et al. (2001) and Gao et al. (2001) have extended their SDVR to directly obtain the three-dimensional wind. The two-scalar technique also includes a provision for hydrometeor fallout and is very computationally efficient, requiring only a few minutes of CPU time on a workstation for a typical three-dimensional grid.

The two-scalar velocity retrieval is applied in the radar coordinate system shown in Fig. 1 of Shapiro et al. (1995a). The retrieval assumes that the three-dimensional distribution of two conserved scalars and the radial velocity is known at three successive time levels. The first scalar is defined to be the log of the radar reflectivity and a simple forcing term accounts for the deviation of the hydrometeor motion from the air motion.

As discussed by Shapiro et al. (1995a) an equation for a second conserved scalar is derived from the first scalar conservation equation by imposing a temporal constraint on the velocity field. Two possible velocity constraints are velocity stationarity and Taylor's frozen turbulence hypothesis (Taylor 1938). Because of the large mean wind component for the supercell case studied herein, it is anticipated that Taylor's frozen turbulence hypothesis is the more appropriate assumption. It states that the local time tendency of the velocity field is assumed to be caused exclusively by advection of a time-invariant pattern of turbulent eddies. Taylor's hypothesis is valid for flows where the turbulent velocity fluctuations represent small perturbations superimposed upon a large translational velocity. It tends to break down in regions of large mean shear. In order to utilize the frozen turbulence assumption to derive a second conserved scalar, suitable velocity pattern translation components must be specified. Following Shapiro et al. (1995a), these components are found from a least squares solution to a radial velocity constraint described by Gal-Chen (1982). The reader is referred to these papers for a detailed discussion of the constraint and the solution procedure, which leads to a pair of coupled cubic equations for the constant pattern translation components.

An additional retrieval constraint is provided by mass conservation, which is expressed in the radar coordinate system as

$$\frac{1}{r^2}\frac{\partial(r^2 v_r)}{\partial r} + \frac{1}{r\cos\theta}\frac{\partial v_\phi}{\partial \phi} + \frac{1}{r\cos\theta}\frac{\partial(\cos\theta v_\theta)}{\partial \theta} = 0. \quad (1)$$

Equation (1) can be exactly satisfied by expressing the unobserved spherical velocity components (v_ϕ and v_θ) in terms of a pseudostreamfunction Q. The expressions for the azimuthal and polar velocities are

$$v_\phi = \frac{\partial Q}{\partial \theta}, \quad \text{and} \quad (2)$$

$$v_\theta = -\frac{1}{\cos\theta}\frac{\partial Q}{\partial \phi} - \frac{1}{r\cos\theta}\frac{\partial}{\partial r}\left(r^2 \int_{\theta_0}^{\theta} \cos\Theta v_r \, d\Theta\right), \quad (3)$$

where the lower limit, θ_0, is potentially a function of r and ϕ. For this study, θ_0 is taken as the lowest radar data level, and a hole-filling procedure is used to fill in any gaps along the integration arc. The hole-filling procedure consists of solving a series of 2D Laplace equations on ϕ–θ surfaces with zero-gradient lateral boundary conditions. It is similar to a 2D Cartesian procedure described in Part II. Substitution of (2) and (3) into the two-scalar conservation equations leads to a pair of inhomogeneous, linear, partial differential equations for the pseudostreamfunction Q. An exact solution to the coupled system is not practical, because the presence of errors in the data would likely lead to a violation of the compatibility condition. A least squares formulation of the problem, however, leads to a Poisson equation for the pseudostreamfunction Q, with Neumann boundary conditions involving known quantities.

b. Use of moving reference frames

Previous studies with Shapiro's algorithm have focused primarily on clear air and low-reflectivity cases (Shapiro et al. 1995a,b). For the present case, which is characterized by a deep-convective storm in an environment with a strong mean wind, the retrieval is modified by applying it in a moving reference frame. As described by Gal-Chen (1982), an appropriately chosen reference frame should maximize the accuracy of the evaluation of the local time tendencies. Furthermore, by shifting the radar observations into a reference frame moving with the storm, the amount of data ''overlap'' between the successive scans can also be maximized. This is important, because centered time differences valid at the middle time can only be calculated where radar data from the first and third volume scans overlap. For a rapidly moving storm and a large time interval between radar scans, the region of data overlap can be much smaller than the precipitation volume. Lazarus et al. (2001) note that for cases with strong vertical shear in the environmental flow, a height-dependent moving reference frame may be optimal.

The relationship between the velocity vectors in a fixed reference frame ($\mathbf{V}_{\text{fix}}$) and a reference frame moving with a constant horizontal speed ($\mathbf{V}_{\text{mov}}$) is

$$\mathbf{V}_{\text{mov}} = \mathbf{V}_{\text{fix}} - U\hat{\mathbf{i}} - V\hat{\mathbf{j}}, \quad (4)$$

where U and V are constant domain translation components. It is easy to verify that the various physical constraints employed in the retrieval are Galilean invariant and hence applicable in a reference frame moving with a constant horizontal speed.

Two least squares methods are available for com-

puting the constant reference frame translation components (U and V) from the single-Doppler radar data. (Note that these components are different than the velocity pattern translation components discussed in section 2a.) The first technique utilizes a procedure described by Gal-Chen (1982) for finding a reference frame that minimizes the time tendencies of a given scalar field. Application of this technique to the reflectivity field produces a reference frame that *moves with the storm.* This ''storm propagation'' reference frame should maximize the overlap of the radar fields among the different volume scans and provide the most accurate evaluations of the reflectivity time derivatives. Difficulties would arise in cases where different echoes were moving in significantly different directions within the same analysis domain. Following Gal-Chen (1982), a cost function is defined by

$$J = \iiint \left(\frac{\partial A}{\partial t} + U\frac{\partial A}{\partial x} + V\frac{\partial A}{\partial y}\right)^2 r^2 \cos\theta \, d\theta \, d\phi \, dr, \quad (5)$$

where A is the radar reflectivity field (dBZ). Setting $\delta J = 0$ yields a pair of algebraic equations that can be solved for U and V.

The second procedure yields a reference frame that moves with the *mean wind.* The advantage of this reference frame is that it effectively reduces the retrieval problem to one of obtaining the unobserved *perturbation velocity.* This would likely be very beneficial in situations where the mean wind represents a substantial portion of the total velocity field. However, difficulties could arise in cases where two regions with opposing flow yield a near-zero mean flow (such as across a front). To use this procedure, we define a cost function as follows:

$$J = \iiint \left(v_r - U\frac{x}{r} - V\frac{y}{r}\right)^2 r^2 \cos\theta \, d\theta \, d\phi \, dr. \quad (6)$$

Setting $\delta J = 0$ yields a pair of algebraic equations that can be solved for U and V.

3. The 17 May 1981 radar dataset

a. Radar data collection

On 17 May 1981, two tornadic thunderstorms moved across the National Severe Storms Laboratory (NSSL) dual-Doppler network. The first storm formed near Pocasset, Oklahoma, and moved northeastward, producing an F2 tornado south of Arcadia, Oklahoma, from 2300–2310 UTC. This storm is the focus of the present study and is hereafter referred to as the Arcadia supercell. A detailed dual-Doppler analysis of the Arcadia supercell has been performed by Dowell and Bluestein (1997, hereafter DB97), and their vector wind fields are used to verify the SDVR. The second storm formed near Rush Springs, Oklahoma and also moved northeastward, producing an F3 tornado near Tecumseh, Oklahoma, and an F4 tornado near Okemah, Oklahoma (Brewster 1984).

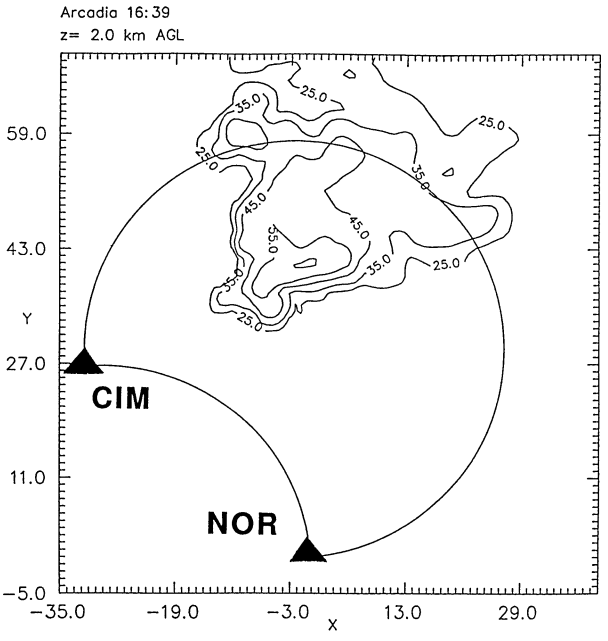

FIG. 2. Locations of the Cimarron, OK (CIM), and Norman, OK, (NOR) radar sites and the crescent-shaped dual-Doppler lobe relative to the Arcadia storm at 2239 UTC 17 May 1981. Contours are radar reflectivity in 10-dBZ increments (starting with 25 dBZ). The grid origin is collocated with NOR and x and y distances are in km.

As the Arcadia supercell moved across the northeast lobe of the NSSL dual-Doppler network, 12 coordinated dual-Doppler scans were obtained with the Norman and Cimarron 10-cm Doppler radars over a 1-h period beginning about 2230 UTC. Figure 2 illustrates the 2239 UTC position of the Arcadia storm relative to the two radars. The northeast dual-Doppler lobe (delineated by between-beam angles of 45° and 135°) is also shown. The Cimarron radar collected data with a range increment of 150 m, an azimuthal increment of ~0.6°, and an elevation angle increment that varied from ~0.5° near the ground to ~3.0° at mid and upper levels of the storm. The Norman radar had similar range and elevation angle increments, but an azimuthal increment of ~1.0°. Both radars had a beamwidth of 0.8°.

For this study, single-Doppler analyses from the Cimarron radar are used as input to the retrieval algorithms, and dual-Doppler analyses from DB97 are used to verify the retrieved wind fields. The raw data from each radar are first manually ''edited'' to dealias the velocity and remove areas of contamination due to ground clutter, sidelobes, and range-folding.

b. Single-Doppler analysis

Following the data editing steps, the reflectivity and radial velocity fields from the Cimarron radar are interpolated from the original radar grid, in which the

azimuthal increments vary slightly, to a new spherical grid on which the SDVR is applied. The new grid has a constant azimuthal increment of $\Delta\phi = 2°$, a constant range increment of $\Delta r = 1$ km, and the original elevation angle increments. A 2D Cressman (1959) algorithm with a circular influence region in the r–ϕ plane is used to map the fields to the new grid.

Because our goal in analyzing fields for input to the SDVR (defined on the new spherical grid) is to retain features with a constant grid-relative wavelength, a special procedure for calculating range-dependent radii of influence is used in the Cressman algorithm. The principle underlying this procedure is to force the radii of influence to be locally isotropic, while allowing the size of the influence region to increase with increasing range to match the variable grid resolution inherent in spherical grids. Using the resultant fields, the SDVR can maximize detail at close range without producing excessive small-scale noise at far range. While appropriate for this application, Trapp and Doswell (2000) caution that nonhomogeneous radii of influence should not be used for studies in which the magnitudes of different radar-analyzed features are compared. Because the analyzed magnitude of a feature is a convolution of the radar observed strength with the analysis weight function, an artificial spatial dependence can be introduced by using spatially varying weight functions.

To obtain expressions for the desired radii of influence, we first define a constant aspect ratio between the radii of influence in the range and azimuthal directions:

$$\alpha = L_r/L_\phi, \tag{7}$$

where L_r and L_ϕ are the radii of influence in the range and azimuthal directions. Local isotropy is enforced by setting $\alpha = 1$, yielding a circular influence region. The physical distances L_r and L_ϕ are related to the corresponding gridpoint distances by

$$L_r = N_r\Delta r, \quad \text{and} \tag{8}$$

$$L_\phi = N_\phi r\Delta\phi, \tag{9}$$

where N_r and N_ϕ are the fractional number of analysis grid points in the range and azimuthal radii of influence, respectively. Next, the product N_rN_ϕ is held constant for all r, resulting in an influence area that increases with increasing radar range. An expression for L_r as a function of range can be derived starting from a general formula for the area of the influence ellipse:

$$\pi L_rL_\phi = \pi rN_rN_\phi\Delta r\Delta\phi. \tag{10}$$

Using (7) to eliminate L_ϕ in (10) and solving for L_r leads to

$$L_r = Kr^{1/2}, \tag{11}$$

where

$$K = (\alpha N_rN_\phi\Delta r\Delta\phi)^{1/2}$$

is constant for all values of radar range.

To utilize this formulation, a physical distance for the range radius of influence is specified for some reference range. Then, N_r and N_ϕ can be calculated for the reference range from (8) and (9). Next, the constant, K, is determined and L_r is calculated for all values of range using (11). As a last step, N_r and N_ϕ are computed for all values of range, using (8) and (9). Note that N_r and N_ϕ apply to the analysis grid, and the physical distances L_r and L_ϕ must be used to determine which radar data points lie within the influence region of a given analysis point. For this study, values of 20 km and 1.8 km were chosen for the reference range and range radius of influence at that reference range.

c. Dual-Doppler verification

Dual-Doppler analyses of the Arcadia supercell from DB97 are used to verify the single-Doppler retrieval results. The reader is referred to DB97 for a detailed description of the analysis procedure; only a brief summary is provided here. First, the raw radar data are interpolated to a common uniform Cartesian grid ($\Delta x = \Delta y = 0.8$ km, $\Delta z = 0.5$ km) using a Cressman (1959) scheme with a spherical influence radius of 1.2 km. In this procedure, data from the lowest elevation angle are extrapolated to the ground. Next, a dual-equation system is iteratively solved in conjunction with a downward integration of the anelastic mass conservation equation to obtain vertical velocities. A boundary condition of $w = 0$ at the top of each data column was used for the downward integration, and an O'Brien (1970) correction was applied to ensure vertical velocities of zero at the ground and data column top.

It is important to note that inaccuracies associated with the assumed upper boundary condition, as well as the extrapolation of data from the lowest elevation angle to the ground, may lead to substantial errors in the computed vertical velocity. Because of these possible errors, quantitative verification of the single-Doppler retrieval against the dual-Doppler analysis is only performed for the azimuthal velocity. Note also that verifying the azimuthal velocity, which is completely unobserved by the ''input'' radar, is more rigorous than verifying the total horizontal wind, which includes a portion of the observed radial velocity.

The verification is accomplished by first trilinearly interpolating both the SDVR and dual-Doppler wind fields to a common unstaggered Cartesian grid. To facilitate the thermodynamic retrieval and model predictions described in Part II of this study, the common grid is chosen to be the scalar points of the ARPS model grid, with constant horizontal and vertical grid spacings of 1.0 km and 0.5 km, respectively. Two quantitative skill scores, the root-mean-square error and the linear correlation coefficient, are then calculated for the retrieved azimuthal velocity.

TABLE 1. Comparison of the moving reference frame translation components (m s^{-1}) calculated from the single-Doppler data with the corresponding verification values for the three successive retrieval times.

Reference frame component	Time 2234 UTC	Time 2239 UTC	Time 2243 UTC	Avg
Storm propagation				
Single-Doppler *U*	7.4	6.9	8.0	7.4
Verification *U*	7.8	8.5	11.4	9.2
Single-Doppler *V*	5.3	5.6	5.7	5.5
Verification *V*	4.9	4.7	5.7	5.1
Mean wind				
Single-Doppler *U*	22.4	22.4	21.9	22.4
Verification *U*	21.6	21.1	21.7	21.5
Single-Doppler *V*	12.9	13.0	13.4	13.1
Verification *V*	14.3	13.4	13.7	13.8

4. Wind retrieval results

a. Skill scores

Utilizing the first five volume scans from the Cimarron radar dataset, three successive wind retrievals are performed to supply three consecutive sets of three-dimensional wind fields for the thermodynamic retrieval (described in Part II). Error statistics for each individual retrieval are presented as well as average statistics for the set of three consecutive retrievals. While the three consecutive retrievals are clearly not independent of each other, examination of the retrieval results at three different times provides insight into the robustness of the retrieval procedure.

Our analysis of the retrieval results focuses on the effects of applying the retrieval in a moving reference frame. Two moving reference frame experiments are considered, one moving with the storm and one moving with the mean wind. Results from these two experiments are compared with results from a fixed reference frame experiment.

Before examining how the two moving reference frames affect the retrieval results, we first evaluate the accuracy with which the reference frame translation components are estimated from the single-Doppler data. As discussed in section 2, simple least squares formulations are used to compute both the storm and mean wind translation components from the single-Doppler data. The estimated storm motion components [reflectivity pattern translation components obtained by minimizing (5)] are verified against subjectively determined storm motion components, while the estimated mean wind components [obtained by minimizing (6)] are verified against mean winds calculated from the dual-Doppler analyses. The estimated and verifying components for each technique, shown in Table 1, indicate that both techniques perform well. Results are especially good for the mean wind components, with average errors less than 1 m s^{-1}.

Table 2 shows the impact of the different moving reference frames on the overall retrieval results. Comparison of rms errors and correlation coefficients for the retrieved azimuthal velocity, as well as the domain maximum vertical velocity, indicates that both moving reference frame experiments perform substantially better than the fixed reference frame experiment. On average, the mean wind reference frame slightly outperforms the storm propagation reference frame. For all reference frames, the retrieved maximum vertical velocities are substantial, but are generally less than half of the magnitude obtained by the dual-Doppler analyses. The reasons for this deficiency will be examined in section 5. Also shown in Table 2 are the skill scores for a simplified retrieval experiment that will be discussed in section 5c.

TABLE 2. Comparison of the three successive wind retrieval skill scores for the different reference frame experiments.

Skill score	Time 2234 UTC	Time 2239 UTC	Time 2243 UTC	Avg
V_ϕ rms error (m s^{-1})				
Fixed frame	7.9	8.1	8.3	8.1
Storm frame	6.1	7.0	6.2	6.4
Mean wind frame	5.5	6.4	6.9	6.3
Simplified retrieval	6.9	7.1	7.3	7.1
V_ϕ correlation coefficient				
Fixed frame	0.47	0.43	0.36	0.42
Storm frame	0.77	0.68	0.71	0.72
Mean wind frame	0.81	0.73	0.65	0.73
Simplified retrieval	0.69	0.67	0.60	0.65
Maximum vertical velocity (m s^{-1})				
Fixed frame	27.8	19.2	23.9	23.6
Storm frame	27.8	20.9	26.3	25.0
Mean wind frame	25.9	24.9	28.1	26.3
Simplified retrieval	27.6	24.3	23.3	25.1
Dual-Doppler verification	63.2	55.8	54.4	57.8

Figure 3 shows the vertical profiles of the azimuthal velocity rms errors for the 2239 UTC wind retrievals. The 2239 UTC retrieval results have been selected for further examination, because they are used to initialize the prediction model and their skill scores best match the three-retrieval average. The errors for the two moving reference frames are generally about 1–2 m s^{-1} less than those for the fixed frame. The only exception is near the storm top, where the mean wind experiment performs significantly better than either of the other experiments.

The vertical profiles of domain maximum vertical velocity for the 2239 UTC retrievals are shown in Fig. 4. All three experiments produce similar profiles, with overall maxima less than half that obtained from the dual-Doppler analysis. The mean wind moving reference frame yields the largest maximum and exhibits the most classic ''bowstring'' profile shape. It is important to note that, because of the vertical velocity assumptions made in the O'Brien correction used in the dual-Doppler analysis, care should be exercised in

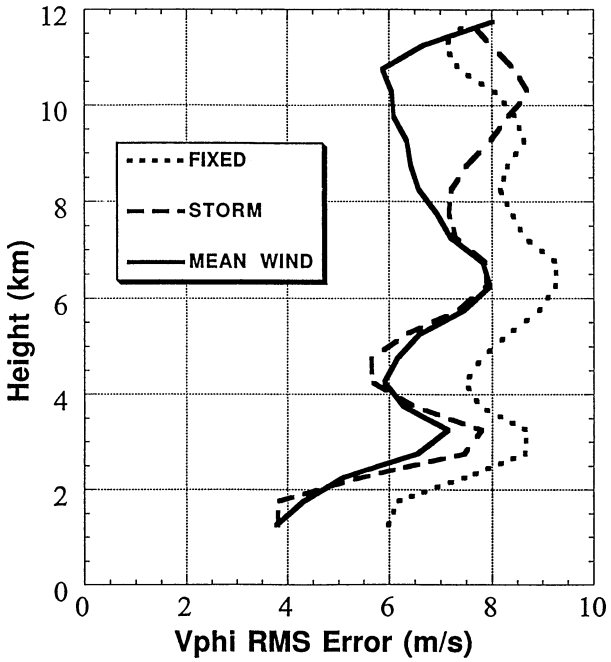

FIG. 3. Vertical profiles of azimuthal velocity rms errors (m s^{-1}) for the 2239 UTC single-Doppler retrieval experiments.

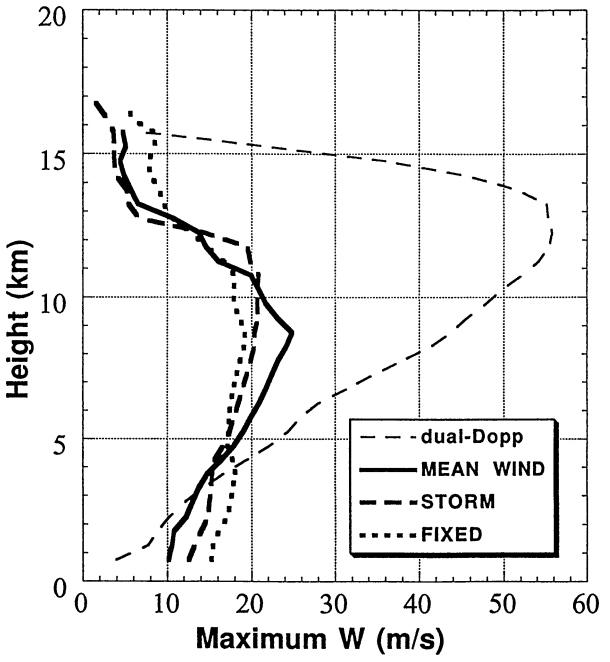

FIG. 4. Vertical profiles of the domain maximum vertical velocity (m s^{-1}) for the 2239 UTC dual-Doppler verification and the single-Doppler retrieval experiments.

directly comparing the retrieved and dual-Doppler vertical velocity fields.

b. Retrieved fields

Individual plots from the 2239 UTC retrievals are now examined to further illustrate the SDVR performance. As noted before, the retrieved fields from this time are used to initialize the numerical predictions presented in Part II of this study. Figure 5 shows the low-level ($z = 2.25$ km) storm-relative vector wind field from the dual-Doppler analysis, and from the three single-Doppler retrieval experiments. Qualitative comparison of the different experiments illustrates the improvement due to the mean wind reference frame. In particular, it best captures the zone of strong storm-relative southeasterly winds northeast of the mesocyclone. This is further illustrated in Fig. 6, a comparison of the retrieved versus dual-Doppler–derived azimuthal velocity. The mean wind experiment best captures the overall azimuthal velocity pattern, as reflected in the superior rmse and correlation scores for this level. Also apparent is the loss of fine-scale detail in all three retrieval experiments.

For the mean wind moving reference frame experiment, the portion of the azimuthal velocity provided to the retrieval by the moving reference frame is

$$\overline{v}_\phi = \hat{\mathbf{e}}_\phi \cdot (U\hat{\mathbf{i}} + V\hat{\mathbf{j}}) = \cos\phi U - \sin\phi V, \quad (12)$$

where U and V are the constant mean wind translation components obtained by minimizing (6). Subtracting this "mean wind" portion of the field from the total retrieved azimuthal velocity yields the retrieved perturbation azimuthal velocity, v'_ϕ. This field represents the portion of the azimuthal velocity obtained solely from the pseudostreamfunction, Q. Figure 7 shows a comparison of the perturbation azimuthal velocity from the dual-Doppler analysis and the mean wind reference frame retrieval. The large region of negative values (southeasterly flow) is successfully retrieved; however, most of the small-scale details are not recovered. Note also that the gradient of the retrieved azimuthal velocity is oriented primarily in the radial direction. This suggests that, within the retrieved field, the magnitude of the azimuthal portion of the polar vorticity, $(1/r)\,[\partial(rv_\phi)/\partial r]$, is greater than the magnitude of the azimuthal portion of the divergence, $(1/r\cos\theta)\,(\partial v_\phi/\partial\phi)$. Confirmation and implications of this inference will be presented in section 5.

Figure 8 shows the perturbation azimuthal velocity fields from the mean wind reference frame retrieval and the dual-Doppler analysis at $z = 10.25$ km. Although the retrieved field is much smoother than the dual-Doppler field, a distinct storm-top divergent velocity couplet is retrieved. Note that in contrast to the low levels where the retrieved perturbation velocity appears to contain little azimuthal divergence, at upper levels the SDVR does yield a qualitatively correct azimuthal divergence signature. The midlevel ($z = 6.25$ km) Cartesian vertical velocity from the mean wind reference frame retrieval and the dual-Doppler analysis are shown in Fig. 9. Again, the retrieved field is significantly smoother than

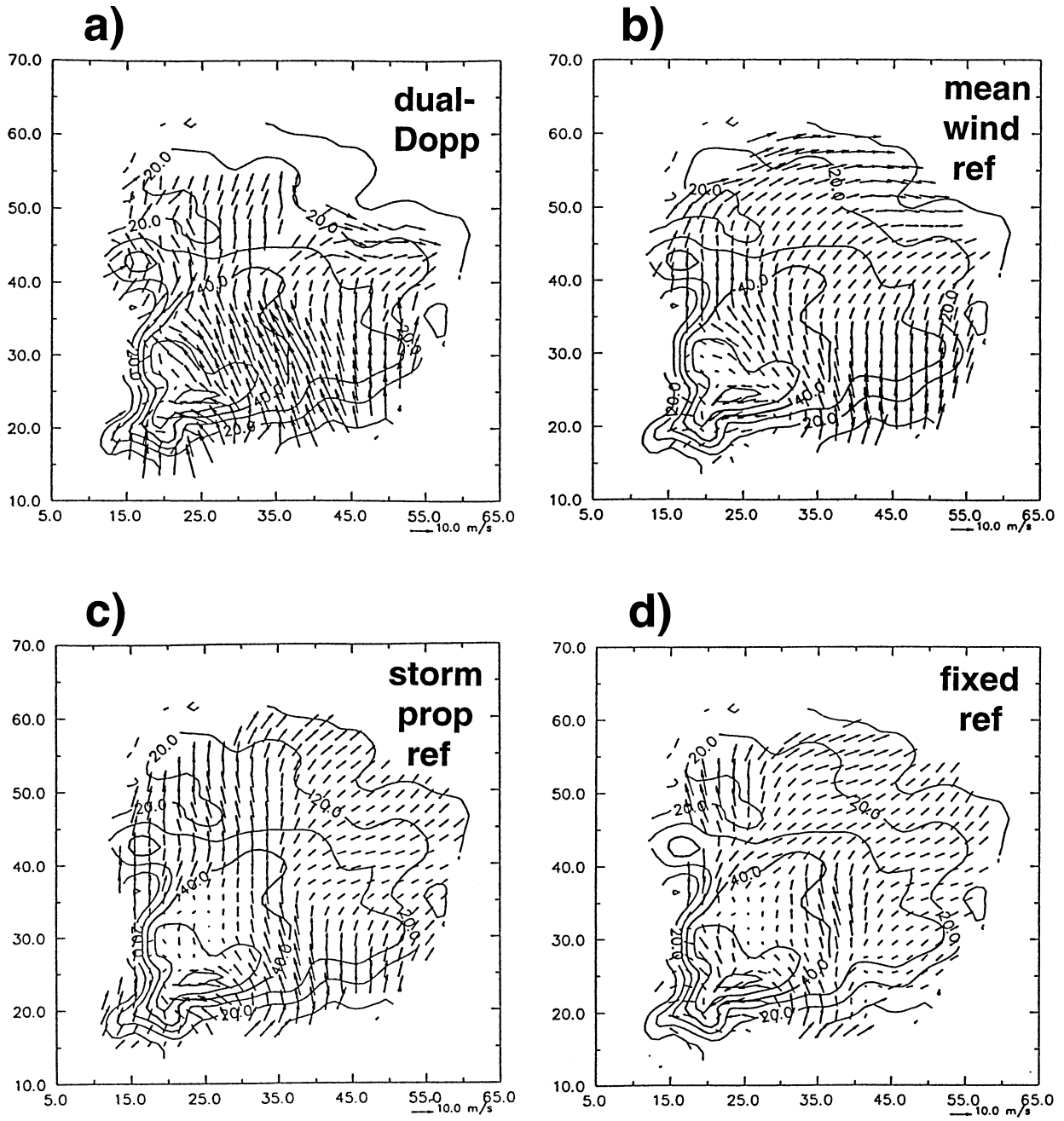

FIG. 5. The 2239 UTC low-level ($z = 2.25$ km) reflectivity and storm-relative horizontal vectors for (a) the dual-Doppler analysis, and the retrieval performed in (b) the mean wind reference frame, (c) the storm propagation reference frame, and (d) the fixed reference frame. Reflectivity is contoured every 10 dBZ. Grid distances are in km and CIM (input) is located at $x = -5$, $y = 10$.

its dual-Doppler counterpart, but captures the principal features reasonably well. In particular, the horseshoe-shaped updraft maximum surrounding the primary vertical velocity minimum is reproduced. The vertical velocity field in the other reference frame experiments (not shown) is remarkably similar to that of the mean wind reference frame retrieval.

5. Analysis of the retrieved wind fields

In addition to illustrating the superiority of the mean wind reference frame retrieval, the results presented in the previous section reveal a number of intriguing features. First, for all three reference frame experiments, the spatial patterns of the retrieved vertical velocity

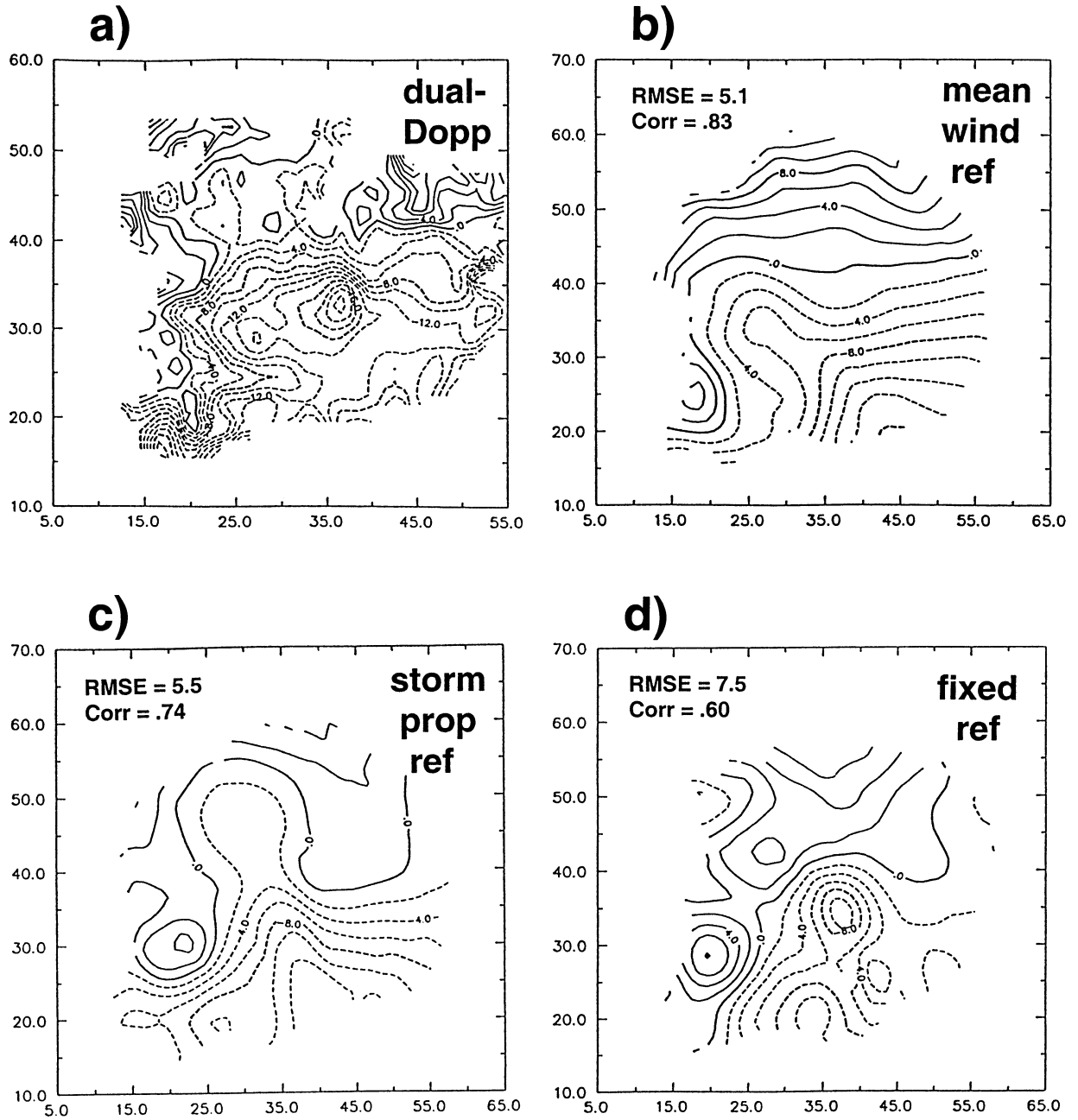

FIG. 6. The 2239 UTC low-level (z = 2.25 km) azimuthal velocity (relative to CIM) for (a) the dual-Doppler analysis, and the retrieval performed in (b) the mean wind reference frame, (c) the storm propagation reference frame, and (d) the fixed reference frame. Azimuthal velocity is contoured every 2 m s^{-1}. Grid distances and radar location are as in Fig. 5.

fields resemble those of the corresponding dual-Doppler analysis quite well, but the retrieved maximum values are significantly smaller in magnitude. Second, while the skill scores for the mean wind reference frame experiment are very good at low levels (z = 2.25 km), qualitative examination of the retrieved perturbation azimuthal velocity suggests that polar vorticity, $(1/r)$ $[\partial(rv_\phi)/\partial r]$, is reasonably well retrieved but azimuthal divergence, $(1/r\ \cos\theta)$ $(\partial v_\phi/\partial\phi)$, is poorly retrieved. Third, near the storm top (z = 10.25 km) the SDVR skill scores are worse than those at low levels; however, a divergent azimuthal velocity couplet is successfully retrieved.

We begin our analysis of the retrieved wind fields by quantifying the qualitative assessments made previously regarding the vorticity and divergence contained within the retrieved perturbation azimuthal velocity. Then, noting that the vertical velocity is kinematically linked to

the vertical profile of horizontal divergence, a vertical velocity decomposition is performed to help explain the vertical velocity results. Finally, results from the full retrieval will be compared with a drastically simplified retrieval suggested to us by the vertical velocity decomposition.

a. Vorticity and divergence calculations

The three-dimensional vorticity vector in radar coordinates is

$$\boldsymbol{\omega} = \hat{\mathbf{e}}_r \frac{1}{r\cos\theta}\left[\frac{\partial(\cos\theta v_\phi)}{\partial\theta} - \frac{\partial v_\theta}{\partial\phi}\right] + \hat{\mathbf{e}}_\phi \frac{1}{r}\left[\frac{\partial(rv_\theta)}{\partial r} - \frac{\partial v_r}{\partial\theta}\right] + \hat{\mathbf{e}}_\theta \frac{1}{r}\left[\frac{1}{\cos\theta}\frac{\partial v_r}{\partial\phi} - \frac{\partial(rv_\phi)}{\partial r}\right] \quad (13)$$

and the three-dimensional divergence, $\nabla\cdot\mathbf{V} = \partial u/\partial x + \partial v/\partial y + \partial w/\partial z$, in radar coordinates is given by (1). For the case of a constant horizontal wind ($\mathbf{V} = U\hat{\mathbf{i}} + V\hat{\mathbf{j}}$), each of the three terms that comprise the three-dimensional divergence will be zero in a Cartesian coordinate system. However, in the radar (spherical) coordinate system, the three terms that sum to give the three-dimensional divergence are not each identically zero. Rather, cancellation occurs between the terms, resulting in a three-dimensional divergence of zero. A similar situation occurs in the calculation of the vorticity components for a mean horizontal wind. In a Cartesian coordinate system, both the vertical component of vorticity and the two terms that comprise it are zero. In contrast, for the radar coordinate system (consider the limiting case of zero elevation angle) the radial and azimuthal contributions to the polar vorticity component are not zero, but cancel each other, resulting in zero polar vorticity. While mathematically correct, these nonzero mean wind terms complicate the interpretation of divergence and vorticity estimates obtained from Doppler radar data. These complications are discussed in the appendix, where it is shown that vorticity and divergence calculations involving spherical velocity components derived from radar observations should be performed using perturbation velocity fields (i.e., fields in which the contribution of the mean horizontal wind to the spherical components is subtracted out prior to the calculations). These mean wind contributions can be seen in the relationship between the total, mean, and perturbation spherical velocities:

$$v_r = \overline{v}_r + v_r' = \cos\theta\sin\phi U + \cos\theta\cos\phi V + v_r', \quad (14)$$

$$v_\phi = \overline{v}_\phi + v_\phi' = \cos\phi U - \sin\phi V + v_\phi', \quad \text{and} \quad (15)$$

$$v_\theta = \overline{v}_\theta + v_\theta' = -\sin\theta\sin\phi U - \sin\theta\cos\phi V + v_\theta'. \quad (16)$$

Using these definitions, we compute the perturbation azimuthal divergence, $(1/r\cos\theta)\,(\partial v_\phi'/\partial\phi)$, and the azimuthal contribution to the perturbation polar vorticity, $(1/r)\,[\partial(rv_\phi')/\partial r]$, for both the mean wind reference frame retrieval and the dual-Doppler analysis. Because the dual-Doppler–derived divergence and vorticity fields are extremely noisy, a five-point smoother is applied to them.

A comparison of the retrieved and dual-Doppler–derived perturbation azimuthal divergence (shown in Fig. 10), confirms that the SDVR obtains very little of the observed low-level perturbation azimuthal convergence.

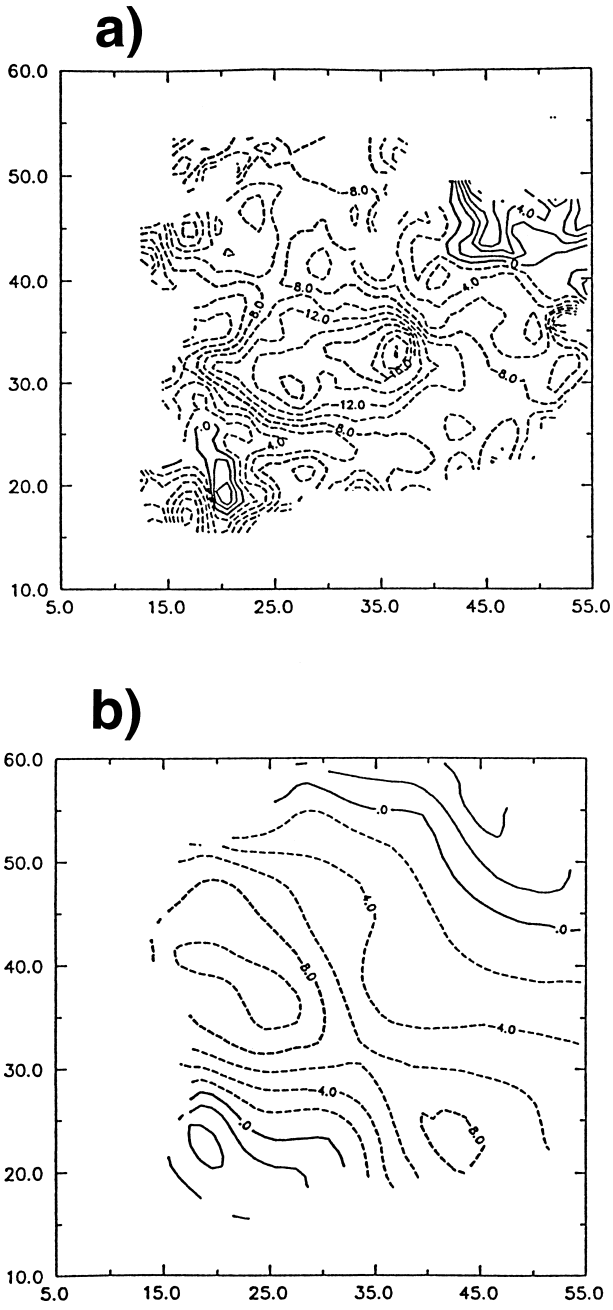

FIG. 7. The 2239 UTC low-level (z = 2.25 km) perturbation azimuthal velocity (relative to CIM) for (a) the dual-Doppler analysis and (b) the retrieval performed in the mean wind reference frame. The contour interval, grid distances, and radar location are as in Fig. 6.

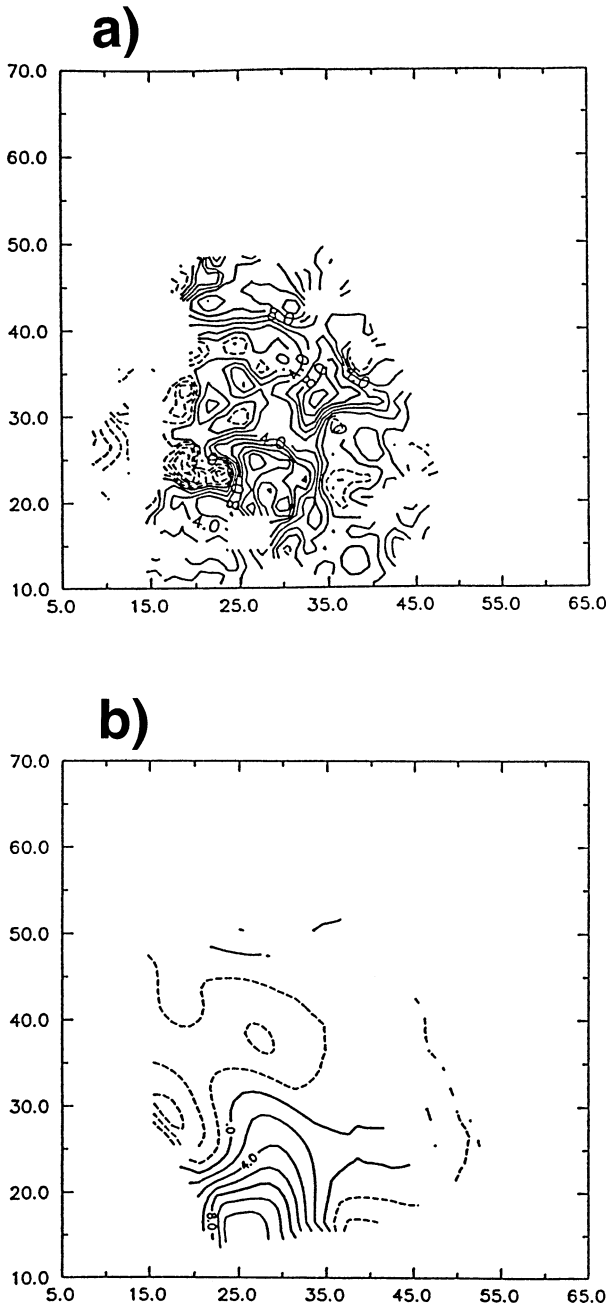

FIG. 8. The 2239 UTC upper-level (z = 10.25 km) perturbation azimuthal velocity (relative to CIM) for (a) the dual-Doppler analysis and (b) the retrieval performed in the mean wind reference frame. The contour interval, grid distances, and radar location are as in Fig. 6.

In fact, the retrieved field shows weak divergence in the southwest portion of the storm, whereas the dual-Doppler verification show strong convergence associated with the low-level inflow into the main updraft. As will be shown, this is consistent with the substantially weaker retrieved updraft maximum compared with the dual-Doppler analysis.

In contrast, the retrieved azimuthal contribution to the perturbation polar vorticity field (Fig. 11b) better matches its dual-Doppler counterpart (Fig. 11a). Note that although the retrieved extrema are smaller than the verification extrema, the zero lines and location of the maximum near $x = 20$, $y = 30$ match quite well. Taken in conjunction with Fig. 3, which shows this level to have nearly the best rms scores, it is concluded that, at low levels, the SDVR retrieves the azimuthal contribution to the perturbation polar vorticity reasonably well, but retrieves very little of the observed perturbation azimuthal convergence.

b. Vertical velocity decomposition

Results from a vertical velocity decomposition are now presented to illustrate the contribution of the retrieved perturbation azimuthal divergence to the retrieved updraft strength. Starting with (1), the expression for mass conservation in radar coordinates, we integrate the r–ϕ divergence in the polar direction to get

$$v_\theta = \frac{\cos\theta_0}{\cos\theta} v_{\theta_0} - \frac{1}{r\cos\theta}\frac{\partial}{\partial r}\left(r^2 \int_{\theta_0}^{\theta} \cos\Theta v_r \, d\Theta\right) - \frac{1}{\cos\theta}\frac{\partial}{\partial\phi}\left(\int_{\theta_0}^{\theta} v_\phi \, d\Theta\right). \quad (17)$$

Defining a mean wind to be that used by the SDVR for the moving reference frame, the radial, azimuthal, and polar velocity components (v_r, v_ϕ, v_θ) can be partitioned into mean and perturbation parts using (14)–(16). Substituting these mean and perturbation parts into (17) and evaluating the integrals involving the mean wind terms (see appendix for details) leads to

$$v_\theta = \frac{\cos\theta_0}{\cos\theta} v'_{\theta_0} - \frac{1}{r\cos\theta}\frac{\partial}{\partial r}\left(r^2 \int_{\theta_0}^{\theta} \cos\Theta v'_r \, d\Theta\right) - \frac{1}{\cos\theta}\frac{\partial}{\partial\phi}\left(\int_{\theta_0}^{\theta} v'_\phi \, d\Theta\right) - \sin\theta(\sin\phi U + \cos\phi V). \quad (18)$$

The Cartesian vertical velocity component can be expressed in terms of the radial and polar velocity components as

$$w = \sin\theta v_r + \cos\theta v_\theta. \quad (19)$$

Substitution of (14) and (18) into (19) leads to an expression for the Cartesian vertical velocity component in terms of the perturbation spherical velocity components,

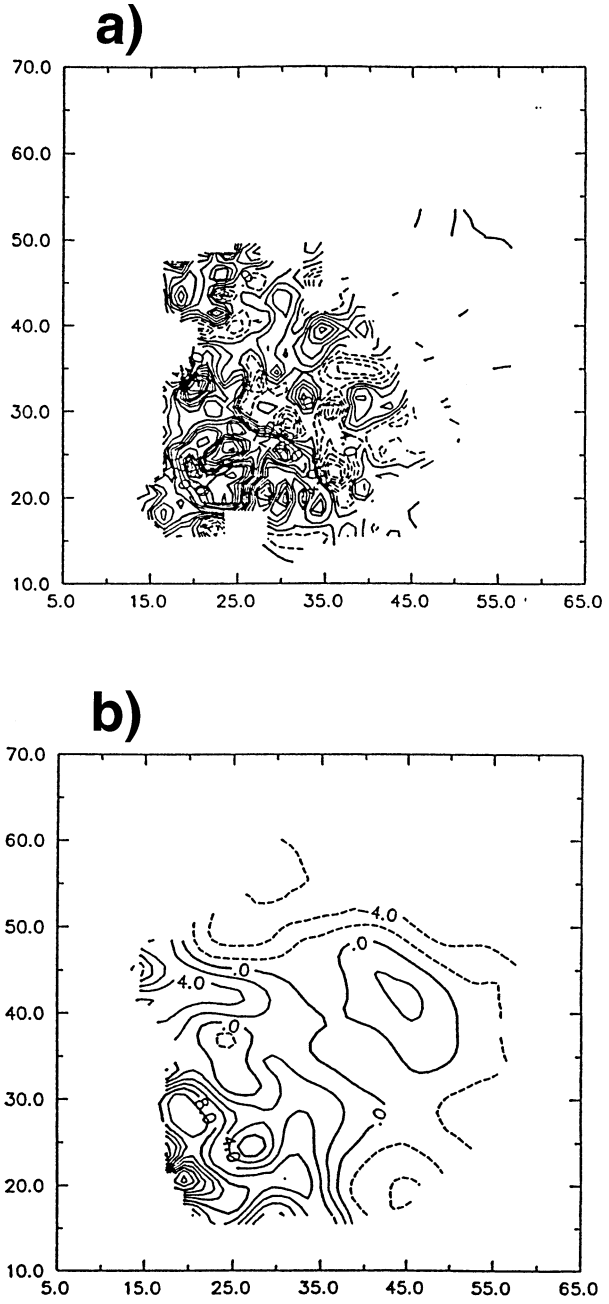

FIG. 9. The 2239 UTC midlevel (z = 6.25 km) vertical velocity for (a) the dual-Doppler analysis and (b) the retrieval performed in the mean wind reference frame. The contour interval, grid distances, and radar location are as in Fig. 6.

$$w = \sin\theta v_r' + \cos\theta_0 v_{\theta_0}' - \frac{1}{r}\frac{\partial}{\partial r}\left(r^2 \int_{\theta_0}^{\theta} \cos\Theta v_r'\, d\Theta\right) - \frac{\partial}{\partial\phi}\left(\int_{\theta_0}^{\theta} v_\phi'\, d\Theta\right). \quad (20)$$

Equation (20) is analogous to the Cartesian expression for vertical velocity in terms of the vertical integral of the horizontal divergence:

$$w = w_{z_0} - \frac{\partial}{\partial x}\left(\int_{z_0}^{z} u\, dZ\right) - \frac{\partial}{\partial y}\left(\int_{z_0}^{z} v\, dZ\right), \quad (21)$$

and is especially relevant to our present analysis of the SDVR results, because it relates the Cartesian vertical velocity to terms involving the observed radial velocity and retrieved cross-beam velocity. The last two terms in (20) are the contributions from the radial divergence (which can be calculated from the observed radial velocity) and the azimuthal divergence (which can be calculated from the retrieved azimuthal velocity). As discussed in the appendix, the terms on the right-hand side of (20) involve only perturbation quantities, because the mean wind portions of these terms have been separated out and summed to zero.

The first term on the rhs of (20) is the vertical projection of the perturbation radial velocity. It can be directly obtained from observed radial velocity (given the estimated mean wind), and is usually small. The second term on the rhs of (20) is the lower-boundary condition for the polar velocity component and is analogous to the lower boundary condition on w in the Cartesian vertical velocity expression. Note that this lower boundary condition is at the lower boundary of the data coverage region, not necessarily at the ground. One of the advantages of the two-scalar retrieval algorithm is that it implicitly obtains this term by directly retrieving a value for the polar velocity at the lowest data level. For retrieval schemes that do not obtain this term (or analogous terms in other coordinate systems), the difficulties of applying boundary conditions above the ground must be faced.

The contribution from each of the divergence terms toward the total retrieved vertical velocity can be computed at any level by integrating upward along an arc of constant range and azimuth. Fortunately, the main updraft in the Arcadia storm has a fairly large horizontal extension, allowing an arc to be found that lies almost entirely within the storm updraft. Figure 12 shows the profiles of the retrieved vertical velocity and the various terms in the decomposition along such an arc. The most striking result is that retrieved vertical velocity is associated almost entirely with the convergence of perturbation radial velocity, which is directly computed from the observed radial velocity (after subtracting the estimated mean wind) in the retrieval. Consistent with Fig. 10, which showed that the retrieval obtains weak azimuthal divergence at low levels, the contribution to the retrieved vertical velocity from the azimuthal divergence term is actually slightly negative at low levels. Note also that the retrieval obtains a reasonable value of about +3 m s^{-1} for the lower boundary condition term.

c. Comparison with a simplified retrieval

The results from the wind decomposition suggest a drastically simplified retrieval against which we now compare the full SDVR. The drastically simplified retrieval retains only those terms that can be directly obtained from the observed radial velocity, and neglects those terms that require solution of the Poisson equation for Q. The various terms can be explicitly written by noting that application of the SDVR in a mean wind moving reference frame is equivalent to performing a perturbation retrieval. Thus (2) and (3) become

$$v'_\phi = \frac{\partial Q'}{\partial \theta}, \tag{22}$$

$$v'_\theta = -\frac{1}{\cos\theta}\frac{\partial Q'}{\partial \phi} - \frac{1}{r\cos\theta}\frac{\partial}{\partial r}\left(r^2\int_{\theta_0}^{\theta}\cos\Theta v'_r\, d\Theta\right), \tag{23}$$

where Q' is a perturbation pseudostreamfunction. Substitution of these expressions into (15) and (16) results in a useful decomposition of the unobserved spherical components:

$$v_\phi = \overline{v}_\phi + v'_\phi = \cos\phi U - \sin\phi V + \frac{\partial Q'}{\partial \theta}, \quad \text{and} \tag{24}$$

$$v_\theta = \overline{v}_\theta + v'_\theta = -\sin\theta\sin\phi U - \sin\theta\cos\phi V - \frac{1}{r\cos\theta}\frac{\partial}{\partial r}\left(r^2\int_{\theta_0}^{\theta}\cos\Theta v'_r\, d\Theta\right) - \frac{1}{\cos\theta}\frac{\partial Q'}{\partial \phi}. \tag{25}$$

Noting that the horizontal mean wind components are obtained from the radial velocity [by minimizing (6)], we see that the simplified retrieval retains all but the final term in each of (24) and (25) (i.e., the terms involving Q'). This simplified retrieval is not offered as an alternative to the full retrieval, but as a reference for assessing the relative contributions from the perturbation pseudostreamfunction and the terms directly obtainable from the radial velocity.

It is important to note that the perturbation radial divergence, the integrand appearing in (25), could be used to obtain a portion of the azimuthal velocity instead of the polar velocity. Thus, while the results of the simple retrieval depend on the direction in which we choose to integrate the radial divergence, the results from the two-scalar retrieval are independent of this choice.

Figure 13a illustrates that the azimuthal velocity obtained by this simple retrieval is merely the local projection of the mean horizontal wind in the azimuthal direction. Consistent with Fig. 12, the retrieved vertical velocity field (Fig. 13b) is very similar to that from the other experiments. Given that the bulk of the vertical velocity is obtained from the perturbation radial convergence, it is now clear why all the experiments obtain similar vertical velocities.

Returning to Table 2, we see that the drastically simplified retrieval clearly outperforms the fixed reference frame experiment. Skill scores for both of the moving reference frame experiments are better, however, indicating that although the mean horizontal wind contains much of the azimuthal velocity field, use of either of the two moving reference frames yields a perturbation azimuthal velocity that adds skill relative to the simplified wind retrieval. In Part II, we assess the effect of these perturbation fields on the subsequent thermodynamic retrieval and numerical prediction.

6. Summary and discussion

In this two-part study, a single-Doppler parameter retrieval technique is developed and applied to a real-data case to provide model initial conditions for a short-range prediction of a supercell thunderstorm. The technique consists of the sequential application of a single-Doppler velocity retrieval, followed by a variational velocity adjustment and a thermodynamic retrieval. In Part I of the study, we have described the SDVR and techniques for applying it in a moving reference frame. Two possible moving reference frames were considered: one that follows the storm motion and one that follows the mean wind. For each of these moving reference frames, we presented simple variational procedures for estimating the horizontal translation components.

The SDVR was used to retrieve the complete three-dimensional wind field within a deep-convective storm from a time series of single-Doppler radar observations. Verification of the retrieved wind fields was accomplished by comparing them with corresponding dual-Doppler analyses. For each of the two moving reference frames considered, the simple variational procedure obtained the horizontal translation components with a high degree of accuracy. Application of the retrieval in either of the moving reference frames significantly improved the results compared with the fixed frame. The best results, however, were obtained for the mean wind moving reference frame, which effectively reduced the problem to one of retrieving the unobserved perturbation velocity. For the mean wind moving reference frame case, the correlation coefficient between the retrieved and dual-Doppler–derived azimuthal velocity (averaged over the entire 3D storm volume) ranged from 0.65 to 0.81 for three successive applications of the retrieval.

A decomposition of the retrieved azimuthal velocity indicated that the projection of the mean wind moving reference frame components accounted for a substantial portion of the total retrieved azimuthal velocity. Subtracting this azimuthal projection of the estimated mean wind from the retrieved azimuthal velocity allowed a comparison of the retrieved and verifying perturbation azimuthal velocity fields. At low levels, the retrieved perturbation azimuthal velocity was associated mostly with polar vorticity, and exhibited weak azimuthal divergence. In contrast, the dual-Doppler verification contained strong azimuthal convergence at low levels. Con-

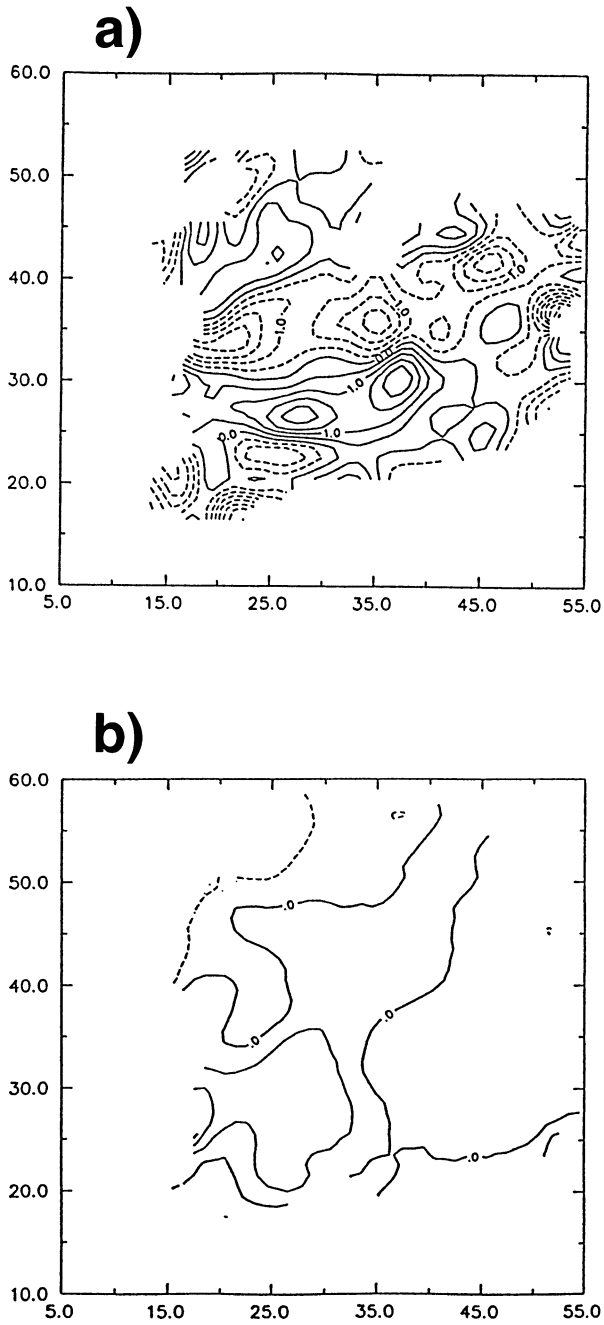

FIG. 10. The 2239 UTC low-level (z = 2.25 km) perturbation azimuthal divergence (10^{-3} s^{-1}) for (a) the dual-Doppler analysis and (b) the retrieval performed in the mean wind reference frame. The contour interval is 0.5 × 10^{-3} s^{-1}. Grid distances and radar location are as in Fig. 5.

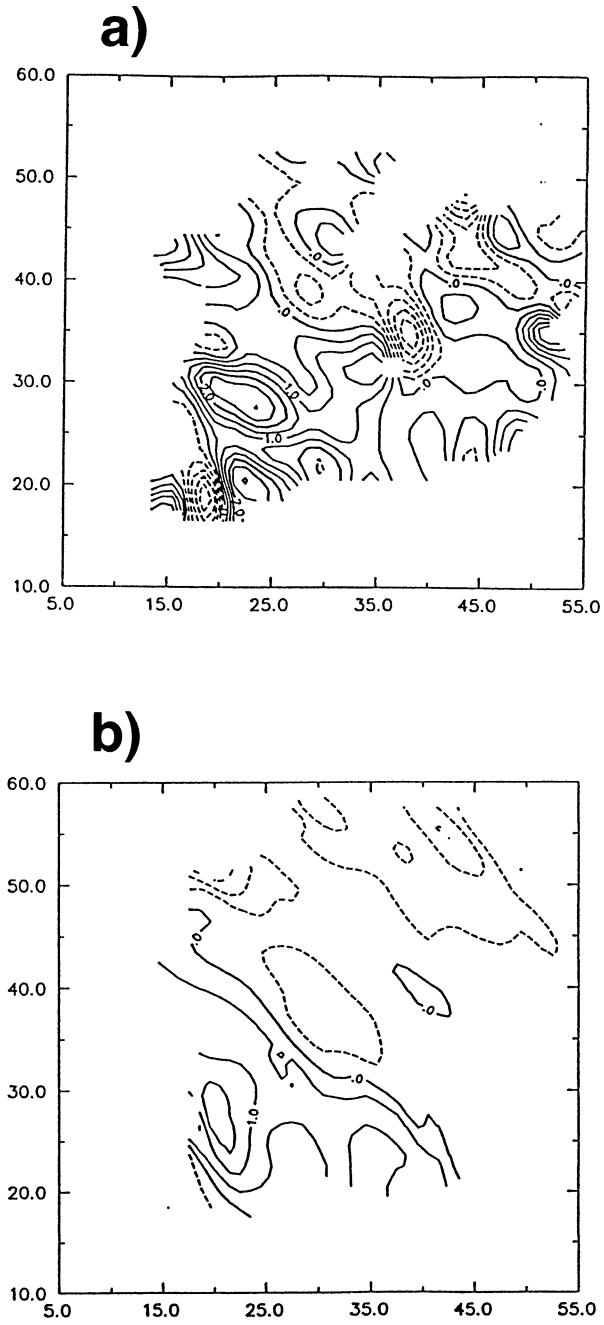

FIG. 11. The 2239 UTC low-level (z = 2.25 km) perturbation azimuthal contribution to polar vorticity (10^{-3} s^{-1}) for (a) the dual-Doppler analysis and (b) the retrieval performed in the mean wind reference frame. The contour interval is 0.5 × 10^{-3} s^{-1}. Grid distances and radar location are as in Fig. 5.

sistent with this, the retrieved updraft maximum of 25 m s^{-1} was slightly less than half of the dual-Doppler observed updraft maximum.

Consideration of these differences led to the introduction of a wind decomposition that illustrates the contributions to the retrieved Cartesian vertical velocity from the various terms in Shapiro's two-scalar technique. Application of this decomposition to the retrieved wind field showed that the bulk of the retrieved updraft was due to the convergence of perturbation radial velocity, which is directly calculated from the radar observations and is used in the wind retrieval. It is not

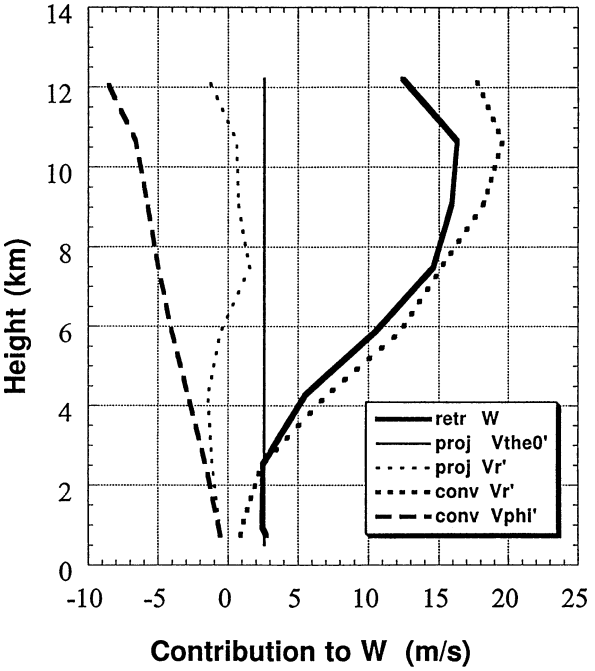

FIG. 12. Vertical profile of the retrieved Cartesian vertical velocity (retr W) along an arc of constant range and azimuth through the main storm updraft. Also shown are the contributions from the four terms on the rhs of (20): the projection of the perturbation radial velocity (proj Vr'), the projection of the lower boundary perturbation polar velocity (proj Vthe0'), and the perturbation radial and azimuthal convergences (conv Vr', conv Vphi'). All profiles are in m s^{-1}.

clear why the wind retrieval failed to capture the observed low-level azimuthal convergence, but we speculate that in this region (where significant condensation is occurring) a strong deviation from reflectivity conservation exists. Consistent with this explanation, the successful retrieval of storm-top divergence (in a region where sublimation is occurring) may be understood by noting that storm-top sublimation likely occurs at a slower rate than low-level condensation.

Recognizing that both the mean wind and the majority of the retrieved updraft were obtained directly from the observed radial velocity, comparisons were made between the fields from the full SDVR and fields obtained from a drastically simplified retrieval. This simplified retrieval consists of the observed radial velocity, estimated mean horizontal wind components, and contribution of the perturbation radial velocity to the polar velocity (obtained from mass conservation). The primary difference between the fields from the simplified retrieval (which omitted the contribution from the pseudostreamfunction) and those from the full retrieval is the polar component of vorticity at low levels.

Although the SDVR performed quite well in this application to a deep-convective storm, further testing is needed for a variety of different storm types and radar scan angles. Of particular importance will be determining the extent to which these optimistic results

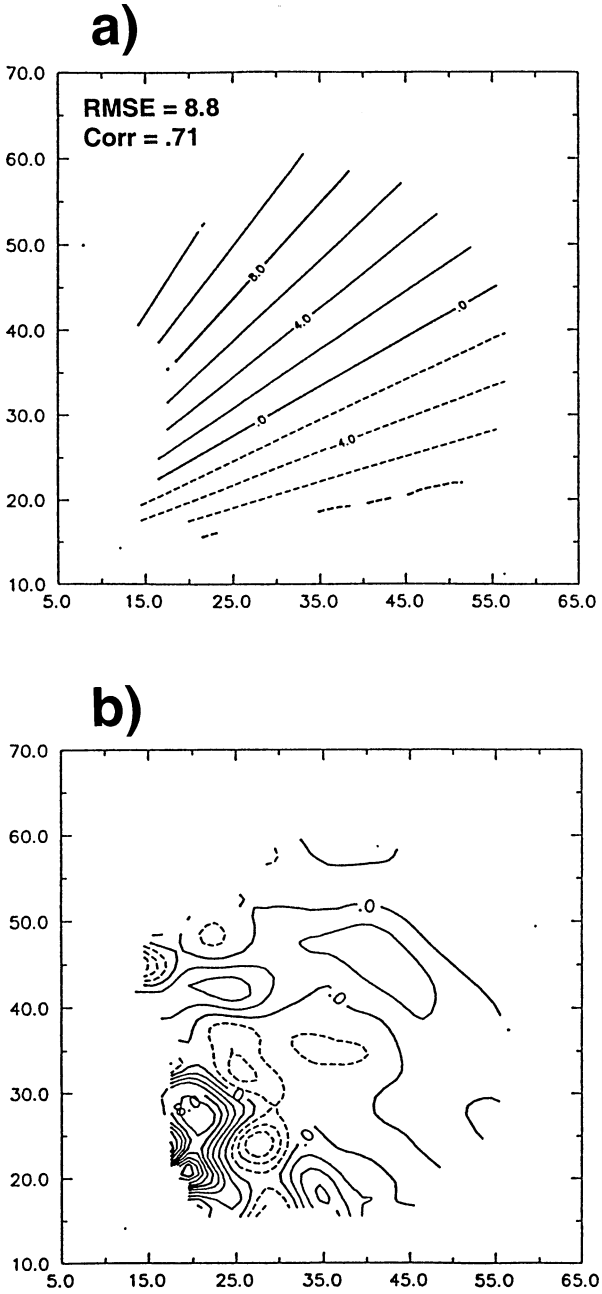

FIG. 13. The 2239 UTC retrieved fields from the simplified velocity retrieval. (a) Low-level (z = 2.25 km) azimuthal velocity and (b) midlevel (z = 6.25 km) vertical velocity. Azimuthal and vertical velocity are contoured every 2 m s^{-1}. Grid distances and radar location are as in Fig. 5.

can be duplicated for more rapidly evolving storms and for scan angles orthogonal to the mean wind or parallel to squall lines. As a complement to real-data experiments, a series of carefully constructed observing system simulation experiments would be helpful in systematically evaluating retrieval performance for a variety of situations.

In Part II of this study, thermodynamic retrieval

and numerical prediction experiments are conducted with the single-Doppler retrieved and dual-Doppler analyzed wind fields. A principal focus will be to compare the thermodynamic retrieval and model prediction results for three sets of wind fields: 1) those obtained from the dual-Doppler analysis, 2) those obtained from the full single-Doppler velocity retrieval applied in the mean wind reference frame, and 3) those obtained from the drastically simplified retrieval described in section 5.

Acknowledgments. We are indebted to Howard Bluestein and David Dowell for providing us with the Doppler radar data and dual-Doppler analyses. The radar data were edited and analyzed using software developed at the National Center for Atmospheric Research. Graphics were created using ZXPLOT, developed by Ming Xue. Sue Weygandt assisted with the preparation of figures. The authors have benefited from discussions with Steve Lazarus, Doug Lilly, Jerry Straka, John Lewis, Fred Carr, Scott Ellis, and Ming Xue. Scientific reviews by Dezso Devenyi and Steve Koch, and a technical review by Nitta Fullerton, are gratefully acknowledged. The research was supported by the National Science Foundation through Grant ATM91-20009 to the Center for Analysis and Prediction of Storms and by a supplemental grant from the FAA. One of us (AS) was also supported by the United States Department of Defense (Office of Naval Research) through Grant N00014-96-1-1112. Computer support was provided by the Environmental Computing Applications System, which is supported by the University of Oklahoma and National Science Foundation under Grant EAR95-12145.

APPENDIX

Horizontal Mean Wind Effects on Divergence and Vorticity Calculations Using Spherical Velocity Components Derived from Radar Observations

Meteorologists have frequently used radial velocity fields obtained from single-Doppler radar sweeps to calculate divergence and vorticity quantities (Roberts and Wilson 1989; Burgess and Lemon 1990; Burgess and Magsig 1998; Funk et al. 1998; Glass and Britt 2000). In most cases, these single-Doppler–derived quantities are used as proxies for the more desirable two-dimensional Cartesian quantities (horizontal divergence and vertical vorticity). The purpose of this appendix is to illustrate how spherical projections of a mean horizontal wind affect radar-computed divergence and vorticity.

We begin by considering a spatially constant horizontal wind, which obviously has no three-dimensional divergence. Furthermore, in a Cartesian coordinate system, each of the three terms in the equation for the three-dimensional divergence is also zero. In a spherical coordinate system, however, the individual terms are not each identically zero; rather, cancellation between the terms occurs, yielding zero three-dimensional divergence. These nonzero terms, while mathematically correct for the spherical coordinate system, complicate the interpretation of divergence estimates obtained from Doppler radar data.

We illustrate this complication by documenting the various mean wind terms in an expression for the Cartesian vertical velocity as a function of the radial, azimuthal, and polar velocity components. This expression, a simplified form of the more general (20), is derived by invoking mass conservation in spherical coordinates and involves polar integrals of the radial and azimuthal divergence. We then show that the sign of the mean wind contribution to the radial divergence term depends on whether the scanned region is upwind or downwind from the radar. As a side note, we demonstrate that the common practice of calculating radial divergence as $\Delta v_r/\Delta r$ (Lemon and Burgess 1980; Witt and Nelson 1984; Wilson et al. 1984; Uyeda and Zrnic 1986; Hermes et al. 1993) has the beneficial property of neglecting the mean wind contribution to the radial divergence, but also neglects another portion of the radial divergence. Next, we show that a similar mean wind effect exists for the calculation of polar vorticity and evaluate its significance. We conclude by recommending a simple procedure for removing these mean wind effects in cases where the radial divergence is taken as a proxy for the horizontal divergence.

Expanding the radial velocity in equation (1), we get

$$\frac{\partial v_r}{\partial r} + \frac{2v_r}{r} + \frac{1}{r\cos\theta}\frac{\partial v_\phi}{\partial \phi} + \frac{1}{r\cos\theta}\frac{\partial(\cos\theta v_\theta)}{\partial\theta} = 0. \quad \text{(A1)}$$

Isolating the V_θ term and integrating in the polar direction with the impermeability condition ($V_{\theta_0} = 0$ at $\theta_0 = 0$) leads to

$$v_\theta = \underbrace{-\frac{r}{\cos\theta}\frac{\partial}{\partial r}\left(\int_{\theta_0}^{\theta}\cos\Theta v_r\, d\Theta\right)}_{\int \frac{\partial v_r}{\partial r}\ \text{term}} \underbrace{-\frac{2}{\cos\theta}\left(\int_{\theta_0}^{\theta}\cos\Theta v_r\, d\Theta\right)}_{\int \frac{2v_r}{r}\ \text{term}} \underbrace{-\frac{1}{\cos\theta}\frac{\partial}{\partial\phi}\left(\int_{\theta_0}^{\theta} v_\phi\, d\Theta\right)}_{\int \frac{\partial v_\phi}{\partial\phi}\ \text{term}}, \quad \text{(A2)}$$

where the individual terms are identified below the equation. Note that the first two terms on the rhs of (A2) come from the radial divergence and the last term comes from the azimuthal divergence. The first term on the rhs of (A2) represents the simple ($\partial v_r/\partial r$) approximation to the radial divergence term.

The contributions from the mean horizontal wind are examined by partitioning the three spherical velocity components into mean and perturbation parts using (14)–(16). Substituting (14) and (15) into (A2) and evaluating the integrals involving the mean wind terms leads to

$$v_\theta = \underbrace{-\frac{r}{\cos\theta}\frac{\partial}{\partial r}\left(\int_{\theta_0}^{\theta}\cos\Theta v_r'\,d\Theta\right)}_{\int \frac{\partial v_r'}{\partial r}\text{ term}} \underbrace{-\frac{1}{\cos\theta}[(\sin\phi U + \cos\phi V)(\sin\theta\cos\theta + \theta)]}_{\int \frac{2\overline{v}_r}{r}\text{ term}} \underbrace{-\frac{2}{\cos\theta}\left(\int_{\theta_0}^{\theta}\cos\Theta v_r'\,d\Theta\right)}_{\int \frac{2v_r'}{r}\text{ term}}$$
$$\underbrace{-\frac{1}{\cos\theta}\frac{\partial}{\partial\phi}[(\cos\phi U - \sin\phi V)\theta]}_{\int \frac{\partial \overline{v}_\phi}{\partial\phi}\text{ term}} \underbrace{-\frac{1}{\cos\theta}\frac{\partial}{\partial\phi}\left(\int_{\theta_0}^{\theta} v_\phi'\,d\Theta\right)}_{\int \frac{\partial v_\phi'}{\partial\phi}\text{ term}}, \tag{A3}$$

where the various mean and perturbation terms have been identified below the equation. Note that the $\int \partial\overline{v}_r/\partial r$ term equals zero and contributes nothing to the polar velocity; however, nonzero mean wind contributions do arise from the $\int 2\overline{v}_r/r$ term and the $\int \partial\overline{v}_\phi/\partial\phi$ term. Thus we can see that the mean wind contribution in the radial divergence arises entirely within the $\int 2v_r/r$ term, and that the simple $\partial v_r/\partial r$ approximation removes the mean wind contribution. Unfortunately, this approximation fails to account for the contribution from the $\int 2v_r'/r$ term.

After evaluating the derivatives for the mean quantities in (A3) and recombining the perturbation radial divergence terms, we substitute (A3) and (14) into (19) to get an expression for the Cartesian vertical velocity in terms of the spherical velocity components:

$$w = \sin\theta v_r' - \frac{1}{r}\frac{\partial}{\partial r}\left(r^2\int_{\theta_0}^{\theta}\cos\Theta v_r'\,d\Theta\right) - \frac{\partial}{\partial\phi}\left(\int_{\theta_0}^{\theta} v_\phi'\,d\Theta\right) \underbrace{-\cos\theta\sin\theta(\sin\phi U + \cos\phi V) - \theta(\sin\phi U + \cos\phi V)}_{\int \frac{2\overline{v}_r}{r}\text{ terms}}$$
$$\underbrace{+\theta(\sin\phi U + \cos\phi V)}_{\int \frac{\partial\overline{v}_\phi}{\partial\phi}\text{ term}} + \underbrace{\cos\theta\sin\theta(\sin\phi U + \cos\phi V)}_{\overline{v}_r\text{ term}}. \tag{A4}$$

Thus we see that cancellation occurs between the mean wind terms and the Cartesian vertical velocity can be accurately calculated by retaining only the perturbation (first three) terms listed in (A4). Furthermore, calculations of the magnitudes of the radial and azimuthal divergence contributions to the vertical velocity will be influenced by the mean wind terms.

The signs and magnitudes of the mean wind terms are interpreted as follows. The $(\sin\phi U + \cos\phi V)$ factor that is common to all terms indicates that the amplitude of the mean wind contribution is maximized when the radar beam is aligned with the mean horizontal wind (and equal to zero when the radar beam is perpendicular to the mean horizontal wind). Considering this maximum magnitude case, the mean wind contribution to the radial divergence terms is

$$w^{\max} = -|\overline{\mathbf{V}}_h|(\cos\theta\sin\theta + \theta). \tag{A5}$$

The first term in (A5) has a maximum magnitude of $0.5|\overline{\mathbf{V}}_h|$ for a radar elevation angle of 45°. For small elevation angles it exhibits a linear increase of about 5% of the mean wind for each 3° of elevation angle

increase. Because this term is offset by the radial projection of the mean wind (a term that is available from single-Doppler observations), it typically is not a problem. The second term in (A5) increases linearly with elevation angle, reaching a maximum of about $1.5|\overline{\mathbf{V}}_h|$ as the radar beam approaches vertical. For typical radar elevation angles it has the same dependency as the first term; however, it is more significant because the offsetting term from the azimuthal divergence is not available from single-Doppler observations. Thus, if the region sampled by the radar is downwind from the radar, the mean wind radial divergence contribution to the estimated vertical velocity will be negative (i.e., downward motion). Conversely, if the sampled region is upwind from the radar, the mean wind term will be positive (upward motion).

Next, we illustrate that a similar cancellation of mean horizontal wind terms occurs for the radial and azimuthal contributions to the polar vorticity. Using (14) and (15) to partition the radial and azimuthal velocities into mean and perturbation parts, the polar vorticity [last term in (13)] can be rewritten as

$$\omega_\theta = \underbrace{\frac{1}{r}(\cos\phi U - \sin\phi V)}_{\frac{\partial \overline{v}_r}{\partial \phi}\text{ term}} + \underbrace{\frac{1}{r\cos\theta}\frac{\partial v_r'}{\partial \phi}}_{\frac{\partial v_r'}{\partial \phi}\text{ term}} - \underbrace{\frac{1}{r}(\cos\phi U - \sin\phi V)}_{\frac{\partial \overline{v}_\phi}{\partial r}\text{ term}} - \underbrace{\frac{1}{r}\frac{\partial (r v_\phi')}{\partial r}}_{\frac{\partial v_\phi'}{\partial r}\text{ term}} \tag{A6}$$

where the mean and perturbation terms have been identified below the equation. As with the divergence calculation, cancellation between the mean horizontal wind contributions occurs in (A6). If, however, only the radial velocity terms are retained, a mean wind contribution will result.

The $(\cos\phi U - \sin\phi V)$ factor in the mean wind terms indicates that the amplitude of the mean wind contribution is maximized when the radar beam is aligned perpendicular to the mean horizontal wind (and equal to zero when the radar beam is parallel to the mean horizontal wind). Considering the maximum magnitude case of the radar beam perpendicular to the mean wind, the mean wind portion of the radial velocity contribution to the polar vorticity is given by

$$\omega_\theta^{\max} = \frac{1}{r}|\overline{\mathbf{V}}_h|. \tag{A7}$$

The $1/r$ factor results in fairly significant values at close range. For example, a 20 m s^{-1} mean wind at a range of 20 km would yield a polar vorticity of 10^{-3} s^{-1}. If the region sampled by the radar is to the left of the mean wind vector, the mean radial wind contribution to the polar vorticity will be positive (i.e., cyclonic). If the sampled region is to the right of the mean wind vector, the contribution will be negative (anticyclonic).

We have shown in this appendix that the presence of a mean horizontal wind will introduce a spatial dependence to vorticity and divergence quantities estimated from individual spherical velocity components. This can be a significant issue for meteorological radar applications, where single-Doppler–derived estimates of radial divergence and vorticity are often used as proxies for their Cartesian counterparts. The resulting dependence of radar-estimated vorticity and divergence quantities on the location of the sampled region relative to the radar can be avoided by removing the projection of the mean horizontal wind from the spherical velocity components. A simple and highly accurate procedure for computing the necessary mean horizontal wind components from radial velocity data is presented in section 2b.

REFERENCES

Brewster, K. A., 1984: Kinetic energy evolution in a developing severe thunderstorm. M.S. thesis, School of Meteorology, University of Oklahoma, Norman, OK, 171 pp.

Burgess, D. W., and L. R. Lemon, 1990: Severe thunderstorm detection by radar. *Radar in Meteorology*, D. Atlas, Ed., Amer. Meteor. Soc., 619–647.

——, and M. A. Magsig, 1998: Recent observations of tornado development at near range to WSR-88D radars. Preprints, *19th Conf. on Severe Local Storms*, Minneapolis, MN, Amer. Meteor. Soc., 756–759.

Cressman, G., 1959: An operational objective analysis system. *Mon. Wea. Rev.*, **87,** 367–374.

Crook, A., 1994: Numerical experiments initialized with radar-derived winds. Part I: Simulated data experiments. *Mon. Wea. Rev.*, **122,** 1189–1203.

——, and J. D. Tuttle, 1994: Numerical experiments initialized with radar-derived winds. Part II: Forecasts of three gust front cases. *Mon. Wea. Rev.*, **122,** 1204–1217.

Dowell, D. C., and H. B. Bluestein, 1997: The Arcadia, Oklahoma, storm of 17 May 1981: Analysis of a supercell during tornadogenesis. *Mon. Wea. Rev.*, **125,** 2562–2582.

Droegemeier, K. K., 1990: Toward a science of storm-scale prediction. Preprints, *16th Conf. on Severe Local Storms*, Kananaskis Park, Alberta, Canada, Amer. Meteor. Soc., 256–262.

——, 1997: Numerical prediction of thunderstorms: Challenges, potential benefits and results from real-time operational tests. *WMO Bull.*, **46** (4), 1–13.

Funk, T. W., V. L. DeWald, and Y. J. Lin, 1998: A detailed WSR-88D Doppler radar evaluation of a damaging bow-echo event on 14 May 1995 over north-central Kentucky. Preprints, *19th Conf. on Severe Local Storms*, Minneapolis, MN, Amer. Meteor. Soc., 436–439.

Gal-Chen, T., 1978: A method for initializing the anelastic equations: Implications for matching models with observations. *Mon. Wea. Rev.*, **106,** 587–606.

——, 1982: Errors in fixed and moving frame of references: Applications for conventional and Doppler radar analysis. *J. Atmos. Sci.*, **39,** 2279–2300.

Gao, J., M. Xue, A. Shapiro, Q. Xu, and K. K. Droegemeier, 2001: Three-dimensional simple adjoint velocity retrievals from single-Doppler radar. *J. Atmos. Oceanic Technol.*, **18,** 26–38.

Glass, F. H., and M. F. Britt, 2000: Close range WSR-88D observations of several tornadic storms. Preprints, *20th Conf. on Severe Local Storms*, Orlando, FL, Amer. Meteor. Soc., 190–193.

Hane, C. E., and B. C. Scott, 1978: Temperature and pressure per-

turbations within convective clouds derived from detailed air motion information: Preliminary testing. *Mon. Wea. Rev.,* **106,** 654–661.

Hauser, D., and P. Amayenc, 1986: Retrieval of cloud water and water vapor contents from Doppler radar data in a tropical squall line. *J. Atmos. Sci.,* **43,** 823–838.

Hermes, L. G., A. Witt, S. D. Smith, D. Klingle-Wilson, D. Morris, G. J. Stumpf, and M. D. Eilts, 1993: The gust-front detection and wind-shift detection algorithms for the terminal Doppler weather radar system. *J. Atmos. Oceanic Technol.,* **10,** 693–709.

Klazura, G. E., and D. A. Imy, 1993: A description of the initial set of analysis products available from the NEXRAD WSR-88D system. *Bull. Amer. Meteor. Soc.,* **74,** 1293–1311.

Laroche, S., and I. Zawadzki, 1994: A variational analysis method for the retrieval of three-dimensional wind field from single-Doppler radar data. *J. Atmos. Sci.,* **51,** 2664–2682.

——, and ——, 1995: Retrievals of horizontal winds from single-Doppler clear-air data by methods of cross-correlation and variational analysis. *J. Atmos. Oceanic Technol.,* **12,** 721–738.

Lazarus, S. M., 1996: The assimilation and prediction of a Florida multicell storm using single-Doppler data. Ph.D. dissertation, University of Oklahoma, 340 pp.

——, A. Shapiro, and K. Droegemeier, 2001: Application of the Zhang–Gal-Chen single-Doppler velocity retrieval to a deep-convective storm. *J. Atmos. Sci.,* **58,** 998–1016.

LeDimet, F. X., and O. Talagrand, 1986: Variational algorithms for analysis and assimilation of meteorological observations: Theoretical aspects. *Tellus,* **38A,** 97–110.

Lemon, L. R., and D. W. Burgess, 1980: Magnitude and implications of high speed outflow at severe storm summits. Preprints, *19th Conf. on Radar Meteorology,* Miami, FL, Amer. Meteor. Soc., 364–368.

Lewis, J., and J. Derber, 1985: The use of adjoint equations to solve a variational problem with advective constraints. *Tellus,* **37A,** 309–322.

Lilly, D. K., 1990: Numerical prediction of thunderstorms—Has its time come? *Quart. J. Roy. Meteor. Soc.,* **116,** 779–798.

Lin, Y., P. S. Ray, and K. W. Johnson, 1993: Initialization of a modeled convective storm using Doppler radar–derived fields. *Mon. Wea. Rev.,* **121,** 2757–2775.

Navon, I. M., X. L. Zou, J. Derber, and J. Sela, 1992: Variational data assimilation with an adiabatic version of the NMC spectral model. *Mon. Wea. Rev.,* **120,** 1433–1446.

O'Brien, J. J., 1970: Alternative solutions to the classical vertical velocity problem. *J. Appl. Meteor.,* **9,** 197–203.

Qiu, C. J., and Q. Xu., 1992: A simple adjoint method of wind analysis for single-Doppler data. *J. Atmos. Oceanic Technol.,* **9,** 588–598.

Ray, P. S., B. C. Johnson, K. W. Johnson, J. S. Bradberry, J. J. Stephens, K. K. Wagner, R. B. Wilhelmson, and J. B. Klemp, 1981: The morphology of several tornadic storms on 20 May 1977. *J. Atmos. Sci.,* **38,** 1643–1663.

Rhinehart, R. E., 1979: Internal storm motions from single non-Doppler weather radar. NCAR Tech. Note NCAR/TN-146+STR, 262 pp.

Roberts, R. D., and J. W. Wilson, 1989: A proposed microburst nowcasting procedure using single-Doppler radar. *J. Appl. Meteor.,* **28,** 285–303.

Roux, F., 1985: Retrieval of thermodynamic fields from multiple Doppler radar data using the equations of motion and thermodynamic equation. *Mon. Wea. Rev.,* **113,** 2142–2157.

Rutledge, S. A., and P. V. Hobbs, 1983: The mesoscale and microscale structure and organization of clouds and precipitation in a mid-latitude cyclone. VIII: A model for the ''seeder-feeder'' process in warm-frontal rainbands. *J. Atmos. Sci.,* **40,** 1185–1206.

——, and ——, 1984: The mesoscale and microscale structure and organization of clouds and precipitation in a mid-latitude cyclone. XII: A diagnostic modeling study of precipitation development in narrow cold-frontal rainbands. *J. Atmos. Sci.,* **41,** 2949–2972.

Shapiro, A., and S. Lazarus, 1993: A modified dynamic recovery technique for cloud-scale numerical models. Preprints, *17th Conf. on Severe Local Storms,* St. Louis, MO, Amer. Meteor. Soc., 455–459.

——, S. Ellis, and J. Shaw, 1995a: Single-Doppler velocity retrievals with Phoenix II data: Clear air and microburst wind retrievals in the planetary boundary layer. *J. Atmos. Sci.,* **52,** 1265–1287.

——, and Coauthors, 1995b: Highlights from a single-Doppler velocity retrieval intercomparison project. Preprints, *Sixth Conf. on Aviation Weather Systems,* Dallas, TX, Amer. Meteor. Soc., 541–546.

Smythe, G. R., and D. S. Zrnic, 1983: Correlation analysis of Doppler radar data and retrieval of the horizontal wind. *J. Climate Appl. Meteor.,* **22,** 297–311.

Sun, J., and A. Crook, 1994: Wind and thermodynamic retrieval from single-Doppler measurements of a gust front observed during Phoenix II. *Mon. Wea. Rev.,* **122,** 1075–1091.

——, and ——, 1996: Comparison of thermodynamic retrieval by the adjoint method with the traditional retrieval method. *Mon. Wea. Rev.,* **124,** 308–324.

——, and ——, 1997: Dynamic and microphysical retrieval from Doppler radar observations using a cloud model and its adjoint. Part I: Model development and simulated data experiments. *J. Atmos. Sci.,* **54,** 1642–1661.

——, and ——, 1998: Dynamic and microphysical retrieval from Doppler radar observations using a cloud model and its adjoint. Part II: Retrieval experiments of an observed Florida convective storm. *J. Atmos. Sci.,* **55,** 835–852.

——, D. W. Flicker, and D. K. Lilly, 1991: Recovery of three-dimensional wind and temperature fields from simulated single-Doppler radar data. *J. Atmos. Sci.,* **48,** 876–890.

Talagrand, O., and P. Courtier, 1987: Variational assimilation of meteorological observations with the adjoint vorticity equations. Part I: Theory. *Quart. J. Roy. Meteor. Soc.,* **113,** 1311–1328.

Taylor, G. I., 1938: The spectrum of turbulence. *Proc. Roy. Soc. London,* **A164,** 476–490.

Thepaut, J., D. Vasiljevic, and P. Coutier, 1993: Variational assimilation of conventional meteorological observations with a multilevel primitive equation model. *Quart. J. Roy. Meteor. Soc.,* **119,** 153–186.

Trapp, R. J., and C. A. Doswell, 2000: Radar data objective analysis. *J. Atmos. Oceanic Technol.,* **17,** 105–120.

Tuttle, J. D., and G. B. Foote, 1990: Determination of the boundary layer airflow from a single Doppler radar. *J. Atmos. Oceanic Technol.,* **7,** 218–232.

Uyeda, H., and D. S. Zrnic, 1986: Automatic detection of gust fronts. *J. Atmos. Oceanic Technol.,* **3,** 36–50.

Verlinde, J., and W. R. Cotton 1990: A critical look at microphysical retrieval algorithms. Preprints, *Conf. on Cloud Physics,* San Francisco, CA, Amer. Meteor. Soc., 453–457.

——, and ——, 1993: Fitting microphysical observations of nonsteady convective clouds to a numerical model: An application of the adjoint technique of data assimilation to a kinematic model. *Mon. Wea. Rev.,* **121,** 2776–2793.

Weygandt, S. S., A. Shapiro, and K. K. Droegemeier, 2002: Retrieval of model initial fields from single-Doppler observations of a supercell thunderstorm. Part II: Thermodynamic Retrieval and numerical prediction. *Mon. Wea. Rev.,* **130,** 454–476.

Wilson, J. W., R. D. Roberts, C. Kessinger, and J. McCarthy, 1984: Microburst wind structure and evaluation of Doppler radar for airport wind shear detection. *J. Appl. Meteor.,* **23,** 898–915.

——, N. A. Crook, C. K. Mueller, J. Sun, and M. Dixon, 1998: Nowcasting thunderstorms: A status report. *Bull. Amer. Meteor. Soc.,* **79,** 2079–2099.

Witt, A., and S. P. Nelson, 1984: The relationship between upper-level divergent outflow magnitude as measured by Doppler radar and hailstorm intensity. Preprints, *22nd Conf. on Radar Meteorology,* Zurich, Switzerland, Amer. Meteor. Soc., 108–111.

Xu, Q., 1996: Generalized adjoint for physical processes with pa-

rameterized discontinuities. Part I: Basic issues and heuristic examples. *J. Atmos. Sci.,* **53,** 1123–1142.

Xu, Q., C. J. Qiu, and J. X. Yu, 1994a: Adjoint method retrievals of low-altitude wind fields from single-Doppler reflectivity measured during Phoenix-II. *J. Atmos. Oceanic Technol.,* **11,** 275–288.

——, ——, ——, 1994b: Adjoint method retrievals of low-altitude wind fields from single-Doppler wind data. *J. Atmos. Oceanic Technol.,* **11,** 579–585.

——, ——, H. D. Gu, and J. X. Yu, 1995: Simple adjoint retrievals of microburst winds from single-Doppler data. *Mon. Wea. Rev.,* **123,** 1822–1833.

——, H. D. Gu, and S. Yang, 2001: Simple adjoint method for three-dimensional wind retrievals from single-Doppler data. *Quart. J. Roy. Meteor. Soc.,* **127,** 1053–1067.

Xue, M., K. K. Droegemeier, and V. Wong, 2000: The Advanced Regional Prediction System (ARPS)—A multiscale nonhydrostatic atmospheric simulation and prediction tool. Part I: Model dynamics and verification. *Meteor. Atmos. Phys.,* **75,** 161–193.

——, and Coauthors, 2001: The Advanced Regional Prediction System (ARPS)—A multiscale nonhydrostatic atmospheric simulation and prediction tool. Part II: Model physics and applications. *Meteor. Atmos. Phys.,* **75,** 161–193.

——, ——, ——, A. Shapiro, and K. Brewster, 1995: *ARPS User's Guide, Version 4.0.,* Center for Analysis and Prediction of Storms, 380 pp.

Zhang, J., and T. Gal-Chen, 1996: Single-Doppler wind retrieval in the moving frame of reference. *J. Atmos. Sci.,* **53,** 2609–2623.

Ziegler, C. L., 1985: Retrieval of thermal and microphysical variables in observed convective storms. Part I: Model development and preliminary testing. *J. Atmos. Sci.,* **42,** 1487–1509.

——, 1988: Retrieval of thermal and microphysical variables in observed convective storms. Part II: Sensitivity of cloud processes to variation of the microphysical parameterization. *J. Atmos. Sci.,* **45,** 1072–1090.

Zou, X. L., I. M. Navon, and J. Sela, 1993: Variational data assimilation with threshold processes using the NMC multilevel primitive-equation model. *Tellus,* **45A,** 370–387.

Zupanski, M., 1993: Regional four-dimensional variational data assimilation in a quasi-operational forecasting environment. *Mon. Wea. Rev.,* **121,** 2396–2408.